RNA Targets and Function of Topoisomerase 3β in Reducing Cellular Stress

Shohreh Teimuri and Beat Suter*

Institute of Cell Biology, University of Bern, Berne, 3012, Switzerland

*Corresponding address: Beat.Suter@unibe.ch

Keywords: Topoisomerase 3β, Drosophila, RNA topoisomerase targets, posttranscriptional gene expression, cellular stress, neurodegeneration, cancer.

Abstract (249 words)

Topoisomerase 3β (Top3β) relaxes DNA and RNA, and its dysregulation is implicated in neurodevelopmental and cognitive disorders. We used a novel protocol without artificial cross-linking to isolate RNA targets of Top3β. The features of the target RNAs show that Top3β is particularly active on long RNAs, RNAs with many splice sites, and RNAs that are localized in large cells. For individual top target mRNAs, we demonstrated that the topoisomerase activity had a strong effect on gene expression in cells where the mRNAs travel over long distances and require strict translational control. The encoded proteins depended on the topoisomerase activity for their proper expression levels and subcellular localization. Lack of Top3β activity stresses neurons, too, affecting the morphology of the neuromuscular junction in adult flies, and it causes premature loss of coordinated movement and aging. Top3β activity affects gene expression of (pre)mRNAs with the same characteristics identified in the Top3β targets and homologs of mRNAs with these characteristics are also preferentially mis-expressed in several neurological diseases and cancers which have been associated with changes in human Top3β. To test whether Top3β can indeed play a role in neuronal health through its effect on RNAs, we tested its role in the expression of the ALS/FTD-associated RNA (G4C2)49 in the Drosophila eye assay. The enzymatic activity of Top3β clearly reduced the neurodegenerative activity of this RNA. Therefore, this study not only identified RNA targets of Top3β but also showed the physiological relevance of the enzymatic activity of Top3β toward its RNA targets.

Introduction

Topoisomerase 3β (Top3β) is an RNA-binding protein (RBP) with dual enzymatic activity toward DNA and RNA (1). Topoisomerases are better known for their activity toward DNA, where they resolve tension and supercoiling. Much less is known about the function of topoisomerases toward RNA. Along with other RBPs, Top3β contributes to mRNA translation, particularly in the nervous system, which is significant for neurodevelopment and psychological and physical well-being (2). Its functional importance is suggested by results that link impaired *Top3β* function to various neurodevelopmental and cognitive disorders (2)(3)(73).

Drosophila melanogaster Top3β possesses the key features of a topoisomerase. The predicted catalytic tyrosine (Tyr, Y) residue is present at position 332 (Y332) and is essential for its topoisomerase activity (4). Top3β topoisomerases distinguish themselves from other topoisomerases by their conserved RNA-binding motif called RGG (Arginine Glycine Glycine) box, which binds to RNAs or proteins. Its paralogue Top3α, a DNA topoisomerase, possesses the catalytic tyrosine residue but lacks the RGG box (4). *In vitro*, the RGG box is not required for the enzymatic activity but might play a role in binding to the RNA and thereby facilitating the enzymatic activity *in vivo* (2).

We hypothesized that the neurological requirements for an RNA topoisomerase might reflect, in part, its activity on mRNAs that need to be transported over long distances to be translated at the right place and at the right time. During such transport, long molecules, such as mRNAs, are likely to become entangled or suffer other structural problems that might interfere with their packaging, transport, unpackaging, and translation (1). A topoisomerase that acts on RNAs might, therefore, be able to rescue such RNAs. As discussed by Su and colleagues (74), there is considerable evidence that Top3β activity on RNA has important functions in cells and that it might act at all levels of gene expression. Using human cell lines, these authors showed that Top3β indeed affects mRNA translation and turnover (74). However, there is still surprisingly little knowledge about the steps in gene expression where Top3β acts on RNAs and particularly about the *in vivo* role of this activity for the cells and the organism. Especially in large cells, where mRNAs need to travel over long distances, an RNA topoisomerase could provide an important advantage and allow

60 the cell to function properly. Drosophila has such large cells in the nervous system, the
61 female germline, and the young, syncytial embryo. The latter is easily accessible and free of
62 additional tissue. The expression of Drosophila Top3β is particularly abundant in 0-2 hours
63 old, syncytial embryos. In these large cells, proper mRNA localization to specific
64 compartments combined with controlled local translation is essential for normal
65 differentiation and cellular physiology. We, therefore, set out to study the activity and
66 function of Drosophila Top3β in young embryos to identify relevant *in vivo* RNA targets,
67 interacting proteins, and biological functions.

68 Consistent with the notion that larger RNAs are more likely to encounter structural
69 problems in living cells, we found that longer RNAs are more likely to be targets of Top3β in
70 young embryos. Specific mutations of the Y332 active site tyrosine (Y332F) and the RGG box
71 (ΔRGG) revealed the importance of the enzymatic activity and the RNA and protein binding,
72 respectively, for the normal function of Top3β. The enzymatic activity of Top3β is needed to
73 bind to mRNAs and for the normal accumulation of these mRNAs and their encoded
74 proteins in general and in specific subcellular locations. We describe evidence that the lack
75 of this enzymatic activity stresses the affected cells and causes neurodegeneration and
76 premature aging. The same RNA features that make an RNA a target of Top3β are also over-
77 represented among the differentially expressed RNAs in the *Top3β* mutants, revealing that
78 such RNAs depend more strongly on the topoisomerase activity. Similarly, these features
79 seem to be overrepresented in misregulated RNAs in many neurodegenerative diseases and
80 cancers with which human *Top3β* had been associated.

81

Results

RNAs depending on *Top3β* for their normal expression

To test whether Top3β affects RNA expression, RNAs from 0-2 hour-old embryos were extracted from a wild-type control strain and the *Top3β* mutants *Top3β*^{26}, *Top3β*^{Y332F}, and *Top3β*$^{\Delta RGG}$. All mutants were both maternally and zygotically mutant. Sequence analysis of the transcriptome carried out on biological triplicates established the effect of the different *Top3β* mutations on the RNA levels expressed in 0-2 hours old embryos. Transcriptome-wide changes in RNA levels between the *Top3β* null mutant *Top3β*^{26} and the wild type were analyzed and RNAs that showed level changes in adjusted p-values <0.05 and absolute log2 fold changes >1 were selected for further analysis (**Supplementary Tables S1, Fig. 1**). This yielded 677 differentially expressed RNAs or which 73% of (496) were downregulated in the null mutant *Top3*^{26}. The effect of *Top3β* on the different RNA levels can either be direct or indirect. Under the assumption that direct effects on RNAs help to rescue RNAs and indirect effects could evenly cause up or downregulation of RNA levels, the estimated number of RNAs directly dependent on *Top3* for their normal expression levels would be around 315.

Gene ontology enrichment analysis on the list of genes that depend on *Top3β* for their normal expression revealed an enrichment for biological processes associated with different aspects of cellular development and physiology (**Supplementary Fig. S1**). Several of these are active in neural processes, including the regulation of axon extension and guidance, and the regulation of synaptic vesicles. This points to the possible effects of Top3β on neuronal processes. We also noted the enrichment of several other processes relating to cellular signaling, regulation of the cytoskeleton, and meta-/catabolic processes.

To investigate the contribution of the catalytic Tyr (which is essential for the enzymatic activity) and the RGG domains (which mediates interactions with RNAs and proteins) to the proper expression of these 677 differentially expressed genes, their expression was also analyzed in both point mutants (**Fig. 1A**). In the *Top3β*^{Y332F} mutant, 220 out of 289 (76%) differentially expressed RNAs were downregulated in the embryos. This fraction is very close to the one of the null mutant, suggesting again, that the majority of these RNAs depend directly on the catalytic activity of Top3β. The impact of the mutated RGG domain on the embryonic transcriptome was less pronounced, with 29 out of 61 (47%) RNAs

downregulated in the embryo, many might be indirect targets. Remarkably, 2 out of 3 of these RNAs depended not only on the RGG motives but also on the Y332 for their normal expression levels.

To focus more on the direct consequences of *Top3β* activity, we selected the embryonic RNAs that depended on *Top3β* for their normal level of expression and were downregulated in the null mutant **(Supplementary Table S1).** We then asked which RNA features were overrepresented in this group compared to the wild-type control. In embryos, the RNAs that were downregulated in the *Top3β*^{Y332F} and *Top3β*^{26} mutants had longer UTRs, CDS, and pre-mRNAs (**Fig. 1B-1D**).

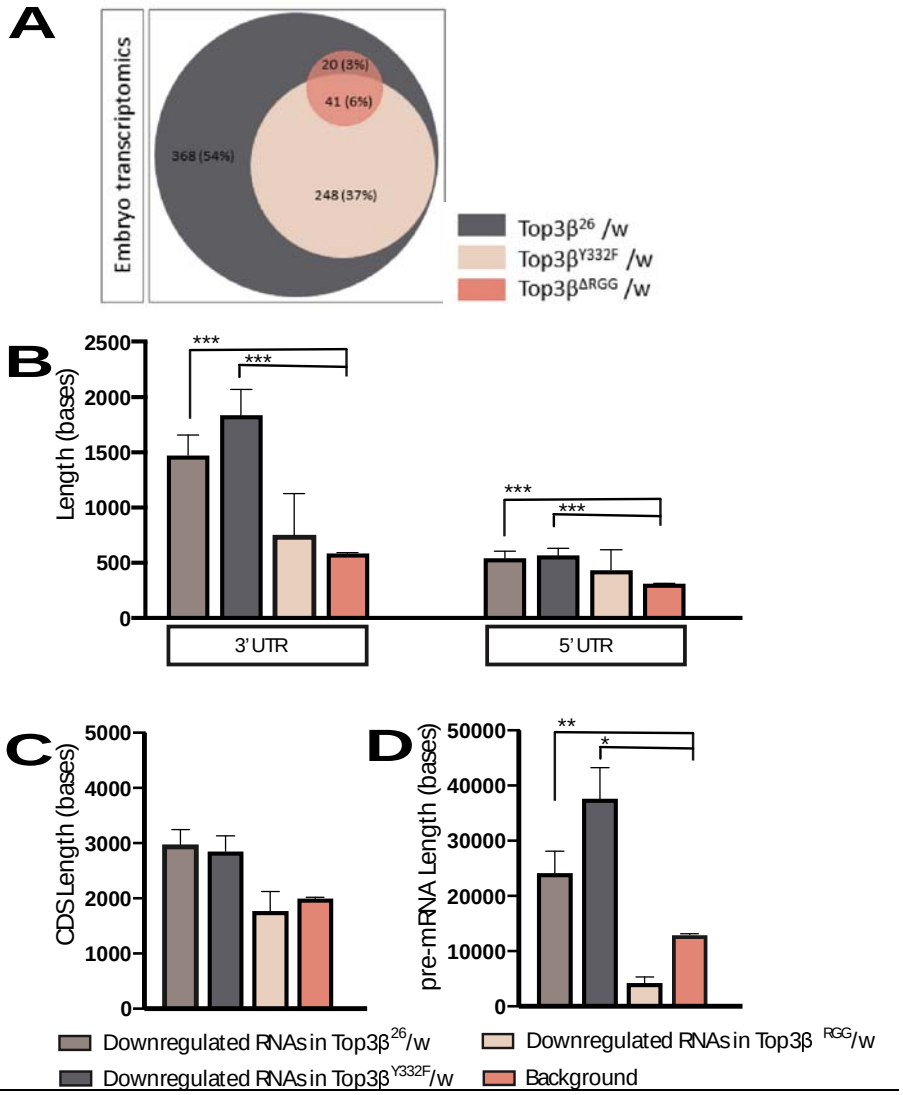

Fig. 1. Effect of the *Top3β* mutations on the embryonic transcriptome. A) Effect of the *Top3β* point mutations on the expression of the 677 genes that are differentially expressed in the *Top3β* null mutant $Top3\beta^{26}$. The number and percentage of differentially expressed RNAs in 0-2 hrs. old embryos are shown. Expression levels were determined relative to the transcript levels of the $Top3\beta^{+}$ strain *w*. **B)-D)** RNA features of transcripts that depend on *Top3β* to reach normal expression levels. **B)** mRNAs with longer UTRs are over-represented in the group of RNAs that depend on *Top3β* to reach normal expression levels. **C)** mRNAs with longer CDS are more downregulated in the $Top3\beta^{26}$ and $Top3\beta^{Y332F}$ mutants. **D)** mRNAs with longer pre-mRNAs are more downregulated in the $Top3\beta^{26}$ and $Top3\beta^{Y332F}$. Expression levels were compared to the $Top3\beta^{+}$ (*w*) control in 0-2 hrs. old embryos. p-value <0.0001=****, p-value <0.001=***, p-value <0.01=**, p-value <0.05=*

Possible roles in neurological diseases and cancers

Top3β has been associated with many neurological diseases and several cancers. If *Top3β* has a general function in allowing the expression of higher levels, particularly of long RNAs, we expect that such RNAs are also more likely to be misregulated in diseases with human *Top3β* aberrations. A list of diseases associated with *Top3β* was retrieved using gene-disease associations (DisGeNET (v7.0)(5)). This list consisted of 12 diseases which were either neurological diseases or cancers. The lists of differentially expressed genes associated with each of these diseases were then obtained from the same database and used to identify their *Drosophila* orthologues from DIOPT Version 9.0 (**Supplementary Table S2**). The list of these *Drosophila* genes was then compared with the list of genes whose embryonic mRNAs are downregulated in the absence of *Top3β* (**Supplementary Table S1**) to identify any genes shared between the two lists (**Fig. 2**). Due to very short list of shared genes with the Juvenile Myoclonic Epilepsy (JME), this disease was not considered for further studies. For the remaining ones, there is a clear overlap between the two datasets and the overlap ranges between 2 and >3 times the calculated random overlap.

Comparing the shared lists between neurological diseases and downregulated embryonic RNAs revealed a single gene, *Rop,* (*Ras opposite*) that is present in every list (**Fig. 2C**). This suggests that the gene *Rop,* which is involved in vesicle release and control of synaptic activity, may be commonly involved or associated with various neurological diseases and that *Top3β* has a role in the production of either *Rop* mRNA or one of its upstream factors (6)(7).

Comparing all the shared lists between cancers and downregulated embryonic RNAs in the *Top3β* mutants, revealed 50 shared genes (**Figs. 2D, E**). Based on the KEGG pathways, some

of these shared genes are only involved in the MAPK (mitogen-activated protein kinase) signaling pathway. The MAPK signaling pathway regulates various cellular processes, including cell growth, proliferation, differentiation, and survival (8), maintaining cellular homeostasis by tightly regulating the timing and intensity of cell division and programmed cell death (9). It thus seems that the MAPK signaling pathway is particularly sensitive to *Top3β* activity.

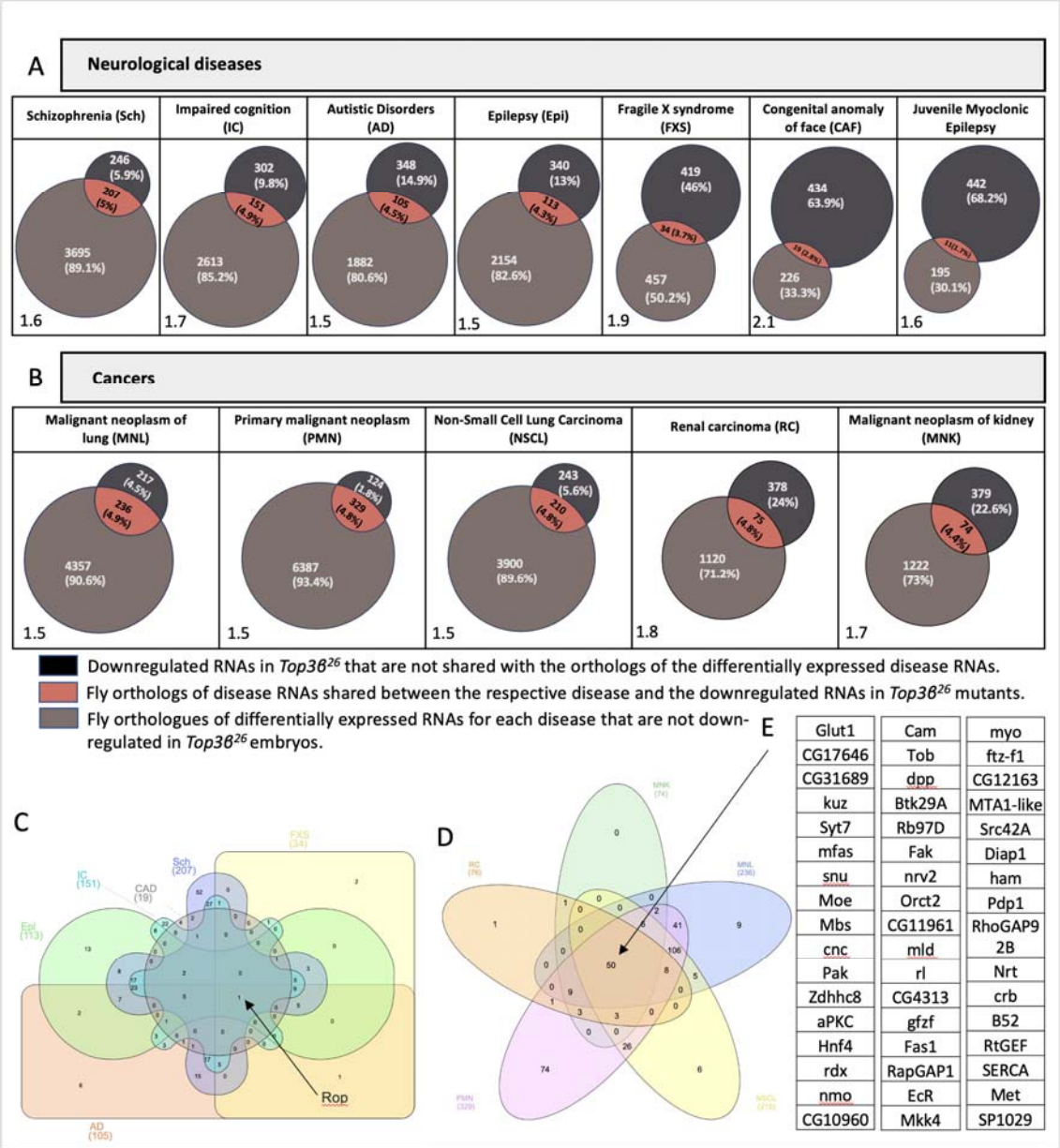

Fig. 2. Overlap between downregulated embryonic RNAs in *Top3β*^{26} and the fly homologs of differentially expressed RNAs in cancers and neurological diseases. A, B) Venn diagram of the genes shared between the list of down-regulated RNAs in *Top3β*^{26} embryos and the fly homologs of differentially expressed RNAs of the listed diseases. Numbers and frequencies are listed. The probability of random overlap is shown in % at the bottom left of each Venn diagram. **C)** Drosophila genes depending on *Top3β* for normal expression levels in embryos were placed into a Venn diagram such that their position shows in which neurological disease their homologs also depend on (human) *Top3β* for their normal expression levels (note that JME was not included). *Rop* appeared in all lists. **D)** Drosophila genes depending on *Top3β* for normal expression levels in embryos were placed into a Venn diagram such that their position shows in which cancer their homologs also depend on (human) *Top3β* for their normal expression levels. **E)** List of the 50 genes that depend on *Drosophila Top3β* for their normal expression levels in embryos and whose homologs are also affected in all listed cancers associated with human *Top3β* alterations.

Comparing the features of the Drosophila RNAs shared between the fly list of embryonic RNAs that depend on *Top3в* to reach proper levels of expression and the homologs of the above human disease datasets revealed that the RNAs shared between the two datasets had on average longer pre-mRNAs and UTRs compared to the RNAs of the individual diseases that were not present in the embryonic list **(Suppl. Fig. S2**). This result is an indication that human *Top3в* might also affect the expression of RNAs with the same features as its fly homolog.

RNA interactions of Top3β

To identify directly the RNA targets to which Top3β binds and performs its topoisomerase activity, we sequenced the RNAs isolated by immunoprecipitation (IP). This was done using animals that expressed an eGFP fused to wild-type Top3β and Top3β in which Y332 was replaced by a phenylalanine (Y332F). During its enzymatic reaction, Top3β forms a covalent bond between its Y332 side chain and the RNA targets (10). Using this to our advantage, we added an ionic detergent at low concentration to the IP, conditions that should pull down primarily covalently bound RNAs without denaturing the antibodies and their interactions. The covalent bond between Top3β's Y332 and the RNA targets was stabilized for the IP by removing Mg^{2+}, which is needed for the enzyme to resolve the bond at the end of the enzymatic reaction (11). To determine if the target RNAs were specifically bound to the –OH group of Y332, we used the Y332F mutant as a negative control, as it does not have this -OH group and, therefore, cannot form the covalent bond. The RNAs that are enriched in the

199 wild type compared to the Y332F mutant are candidate targets of the catalytic activity of
200 Top3β **(Supplementary Table S3)**. Because long RNAs seem more likely to depend on this
201 enzymatic activity, we further tested the quality of the data by comparing the RNA length of
202 the presumed targets with the background RNA length and found that longer RNAs were
203 more likely to covalently bind to Top3β as they showed higher enrichment in the wild-type
204 embryonic extracts compared to the *Top3β*^{Y332F} mutant extracts (**Fig. 3A**). The results might
205 also reflect that longer RNAs have a higher chance of enduring physical stress and are also,
206 for this reason, more likely to become substrates of the enzymatic activity of Top3β.
207 Interestingly, recent work in human cells also found that TOP3β preferentially binds to long
208 mRNAs (74).

209 From the list of immunopurified RNAs, the ones with an adjusted p-value smaller than 0.05
210 (adjp-value<0.05) and a log2-fold change of more than 1 (log2FC>1) were selected and
211 ranked based on their adjp-value. These 46 embryonic RNAs and their genes were used for
212 further analyses (**Supplementary Table S4**). We next analyzed which RNA features correlate
213 with the chance of becoming a target of Top3β's enzymatic activity. The results showed that
214 embryonic Top3β RNA targets had on average longer 3'UTRs and stemmed from larger
215 genes with longer introns compared to the complete set of different types of RNAs detected
216 in the wild-type RNA-IP (**Fig. 3B-C, Supplementary Tables S3, S4)**. The fact that targeted
217 mRNAs have longer 3'UTRs is consistent with mRNAs that undergo localization and/or
218 translational regulation having a higher chance of becoming a Top3β target because these
219 processes are mainly controlled by sequences in the 3'UTR. A higher abundance of mRNAs
220 with long coding sequences (CDS) might reflect that mRNAs with long open reading frames
221 (ORFs) might become a Top3β target when their translation becomes blocked. Embryonic
222 Top3β targets had also a higher number of transcript isoforms per gene and more exons
223 (**Fig. 3D-E, Supplementary Tables S3, S4)**. This might indicate that mRNA splicing, a nuclear
224 activity, increases the chance of an RNA becoming a Top3β target. In summary, these results
225 present the first evidence for the involvement of Top3β in mRNA splicing, mRNA
226 localization, and/or translational control and translation.

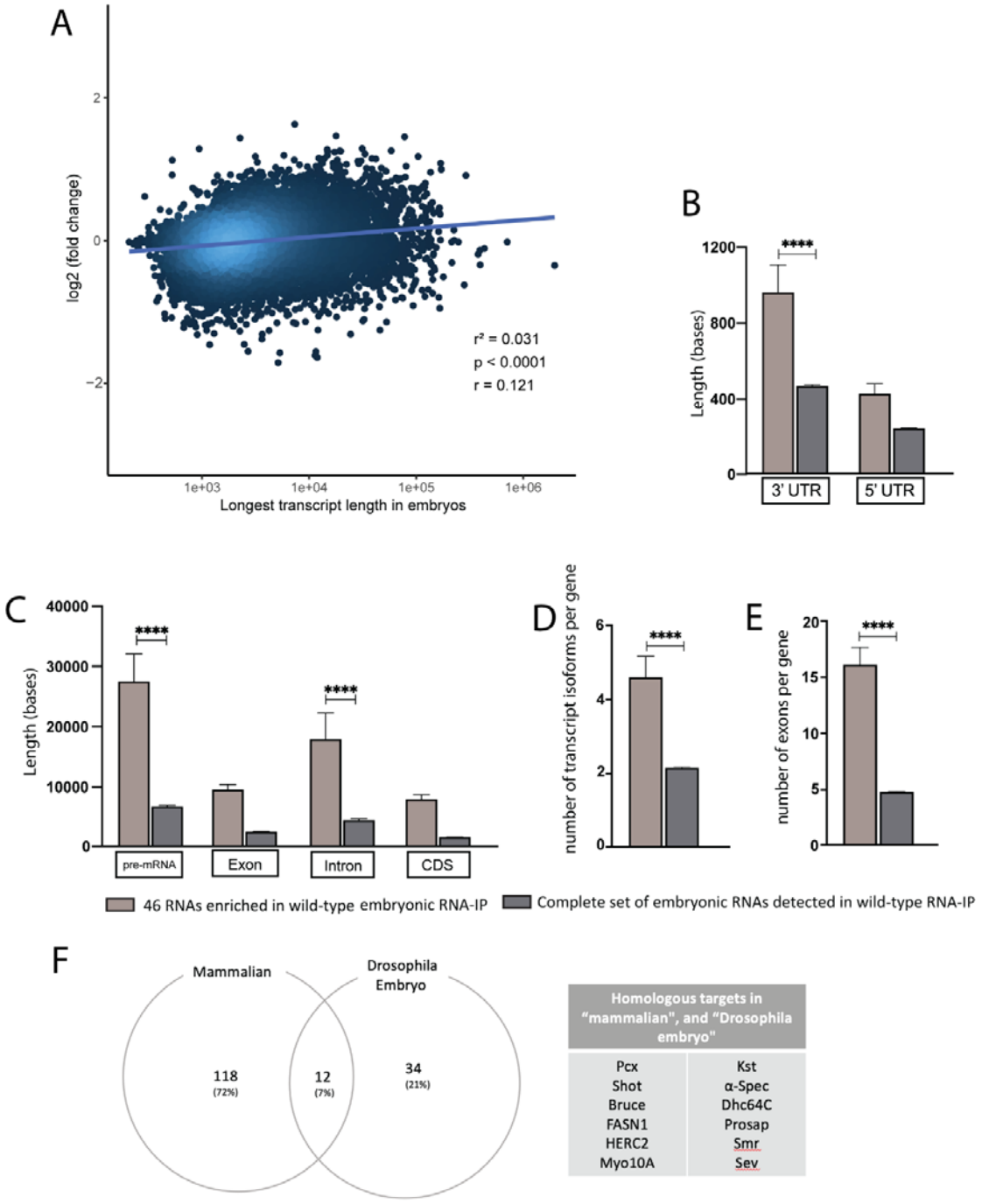

Fig 3: **Characteristics of embryonic RNA targets of Top3β**. **A)** Longer RNAs are more likely targets of the enzymatic activity of Top3β because they are more enriched in the IP with the wild-type Top3β compared to the Top3β^{Y332F}. r measures the strength of the correlation and p stands for p-value. **B-E)** Transcript features of the top 46 embryonic RNA targets of Top3β. The complete sets of RNAs detected in the wild-type RNA-IP served as the standard. p-value <0.0001=****, p-value <0.001=***, p-value <0.01=**, p-value <0.05=*. **F)** Homologous targets shared between Drosophila Top3β and mammalian FMRP1 and Top3β. Venn diagram for the RNAs shared between our study with the previous mammalian study (1), which revealed the overlap of the interactors with mouse FMRP1 from brain extracts and Top3β interactors in HeLa cells. The list of the Drosophila homologs that were also found in both mammalian interactor screens is also shown.

238 **Homologs of Drosophila Top3β target mRNAs bind also mammalian Top3β and FMR1**

239 Mammalian FMRP/FMR1 binds to ribosomes and regulates translation. Comparing our
240 Top3β RNA-IP results with those obtained from the shared targets of FMRP (HITS-CLIP data
241 of FMRP produced from mouse brain extracts) and Top3β (HITS-CLIP data of Flag-Top3β
242 from HeLa cells; (1)) revealed intriguing similarities. A Venn diagram illustrates the overlap
243 between the top targets of Drosophila Top3β and the shared mammalian targets, with the
244 number of such overlapping targets listed in **Fig. 3F**. The common feature of the proteins
245 encoded by the shared RNA targets is that they are predominantly large proteins. Many are
246 localized to the plasma membrane or the cell cortex (e.g., Sev, Mgl, α-Spec, Kst, Pcx) or
247 cytoskeleton-associated (e.g., Dhc64C, Mhc, Myo10A, α-Spec, Kst), have axonal functions
248 (e.g., Shot, Dhc64C, Kst, Prosap), or scaffolding functions (Shot, Prosap). Consistent with
249 similar results in vertebrates (74), these results show that there is a clear overlap between
250 the Top3β and the FMRP activities but, additionally, the two proteins perform activities
251 independent of the other one.

252

253 **Interaction network of the RNA Top3β**

254 To identify proteins that might contribute to the Top3β activity, immunoprecipitations (IP)
255 on extracts from 0-2 hours old embryos were performed using *Top3β-eGFP* and the *eGFP*
256 control line. Polypeptide components of the IP complexes were analyzed using mass
257 spectrometry (MS) and their abundance was compared to the eGFP control. This resulted in
258 a list of 426 potential complex components with an adjusted p-value <0.01 and log2FC >1
259 (**Supplementary Table S5).** With 89, ribosomal proteins were particularly highly represented
260 in this set. A gene ontology enrichment analysis was then performed for the top 100
261 (according to log2FC) non-ribosomal proteins **(Fig. 4A)**. This revealed enrichment for
262 proteins involved in the activation of translation, P-bodies, stress granules, and neural
263 ribonucleoprotein granules, all membrane-less structures involved in storing specific mRNAs
264 during periods of stress or concentrating mRNAs and regulatory proteins (12). Additionally,
265 the interactors were also enriched in several functions related to mitochondria.

266 Tdrd3, a well-known interactor of Top3β (13), was among the top enriched proteins,
267 suggesting that our immunoprecipitation was specific. To assess the role of the Y332 residue

and the RGG box in Top3β interactions, we compared the IP results with the ones from the *Top3β* mutants *Top3β*^{Y332F}*-eGFP* and *Top3β*$^{\Delta RGG}$*-eGFP*. Among the 337 non-ribosomal binding candidates, 102 needed the Y residue and the RGG box to bind to Top3β-eGFP because they were not enriched in the protein-IP from either mutant **(Supplementary Table S5)**. An additional 16 proteins needed the Tyr (but not the RGG) and 23 the RGG box (but not the Y332) for their binding to Top3β.

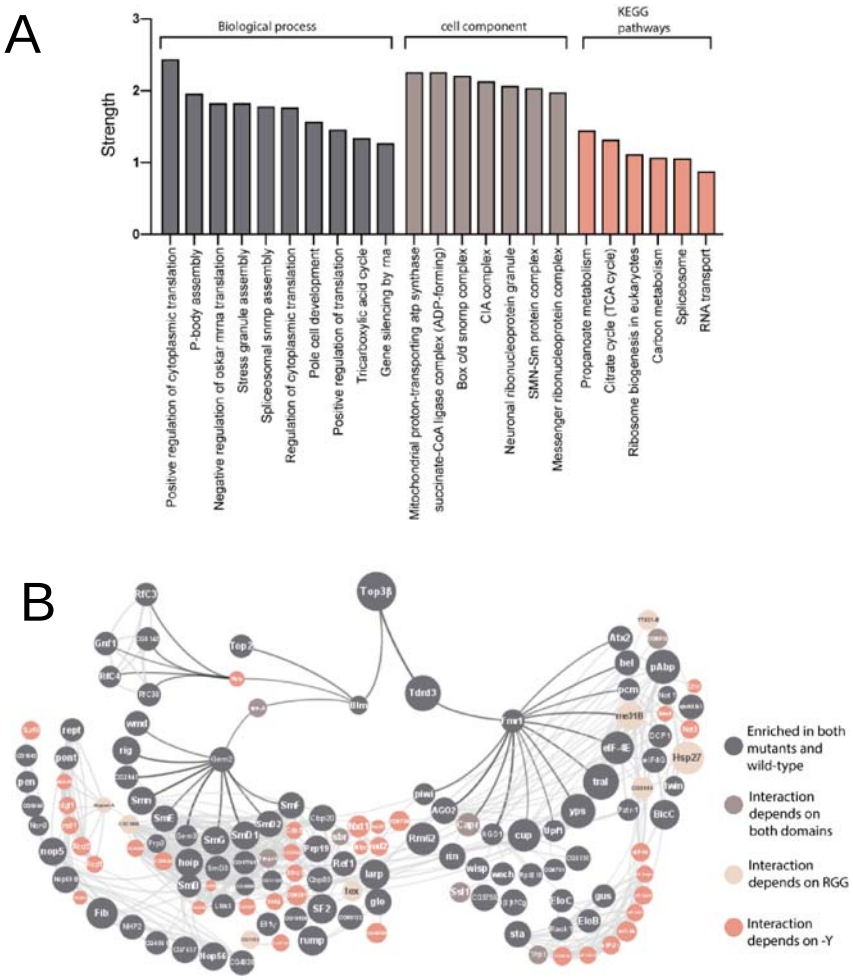

Fig. 4: Pathways and interactions of Drosophila Top3B. A) Gene ontology enrichment for Top3β-associated proteins for the top 100 interactors identified in embryonic extracts. **B)** Proteins enriched in the embryonic protein-IP with their physical interactions according to Cytoscape-String. Proteins that ended up further away from Top3β than the ones shown here, were removed from the interaction map.

280 A large fraction of the identified proteins are involved in RNA transport, translation, splicing,
281 mRNA surveillance, and degradation. A physical interaction map of the proteins enriched in
282 the Top3β::GFP IP was created using Cytoscape-String and the results from the mutant
283 analyses were entered into this map (**Fig. 4B)**. The resulting map resolved into two distinct
284 sub-maps. The left branch connects Top3β functions to its nuclear functions and includes
285 splicing factors. The right branch is enriched in cytoplasmic proteins and includes Tdrd3,
286 FMR1, the piRNA pathway, and translation. The association first with Tdrd3 and at the next
287 level with FMRP shows the strong conservation of the Top3β activities between vertebrates
288 and invertebrates because similar results have been described from work with vertebrate
289 cell cultures (74). The interaction of Me31B with Top3β turned out to be dependent on the
290 RGG box. As an RNA helicase, Me31B is a core component of a variety of ribonucleoprotein
291 complexes (RNPs) that participate in translational control and mRNA decapping during
292 embryogenesis, oogenesis, neurogenesis, and neurotransmission
293 (14)(15)(16)(17)(18)(19)(20)(21). Me31B RNPs also containing Tral, eIF4E1, Cup, and pAbp,
294 are also involved in RNA localization and translational control of maternal mRNAs during
295 oogenesis and embryogenesis (18). These other complex proteins were also enriched in the
296 embryonic Top3β-eGFP IP.

297

298 **Biological relevance of the topoisomerase activity**

299 The *Top3β*^{Y332F} and *Top3β*^{26} mutants have reduced or no function, but the mutations cause
300 neither lethality nor sterility. This is a common phenomenon observed with genes and
301 proteins that are still important for optimizing cellular physiology. In a lab setting, the
302 reduced function of these mutants can often be compensated for by other mechanisms.
303 However, by directly analyzing the cellular phenotypes of the mutants, one may observe
304 increased cellular stress and changes in physiology or anatomy that reveal the cellular
305 function of the normal gene. Such cellular stress and changes often lead to signs of
306 premature aging, like a decline in neuromuscular performance and a shorter lifespan.

307 ***Role of Top3β for localizing and expressing its transcript targets***

308 To evaluate the consequences of the interaction of Top3β with its RNA targets, we selected
309 5 genes (*shot*, *Pfrx*, *Hers*, *Dhc64C*, and *kst)* from the top list of RNAs covalently bound to

310 Top3β for further analysis. These RNAs exhibit several distinctive features, including a high
311 number of transcript isoforms, long mRNAs, localized mRNAs, and maternal expression.
312 *shot*, *Dhc64C* and *kst* homologs were also identified by a mammalian study (Fig. 3; (1)) and
313 they are also expressed in neurons (22)(23). In normal young embryos, *shot* mRNA
314 accumulates more strongly in the polar granules and the pole cells at the posterior end (**Fig.
315 5)**. In embryos that were maternally and zygotically mutant, *shot* mRNA levels were overall
316 reduced and the more intense localized staining pattern in the posterior pole region was
317 lost in the null- and the enzymatic *Top3β*^{Y332F} mutant, but not in *Top3β*$^{\Delta RGG}$, suggesting that
318 the normal expression and localization depends on *Top3β* and particularly on its enzymatic
319 activity. Analogous studies revealed that the anti-Shot antibody signal was weaker in the
320 entire null mutant and *Top3β*^{Y332F} embryos compared to the wild type (**Fig. 5)**, suggesting
321 that the reduced mRNA levels caused the reduced Shot protein expression. These findings
322 are consistent with *shot* mRNA being the primary target of Top3β and they highlight the
323 importance of the enzymatic activity of Top3β for the efficient expression and localization of
324 the encoded protein. In the *Top3β*$^{\Delta RGG}$ mutant embryos, the Shot protein levels, and
325 localization were also less affected, as the mRNA levels were **(Fig. 5)**. The effect on the
326 proteins encoded by two more *Top3β* targets were similar. The cytoplasmic Dynein heavy
327 chain (Dhc or Dhc64C) protein accumulated more strongly at the posterior end of the wild-
328 type embryo, in front of the pole cells. This was neither detectable in the null mutant nor in
329 *Top3β*^{Y332F} **(Fig. 5)**. The Kst protein accumulated at the apical cortex in normal blastoderm
330 embryos, but in the *Top3β* null mutant and *Top3β*^{Y332F} its signal was reduced throughout the
331 embryo, including the apical cortex. Protein signals for Dhc and Kst showed an intermediate
332 level in the *Top3β*$^{\Delta RGG}$ mutant embryos **(Fig. 5)**, indicating that the RGG box also affects their
333 expression, albeit less strongly than the catalytic activity.

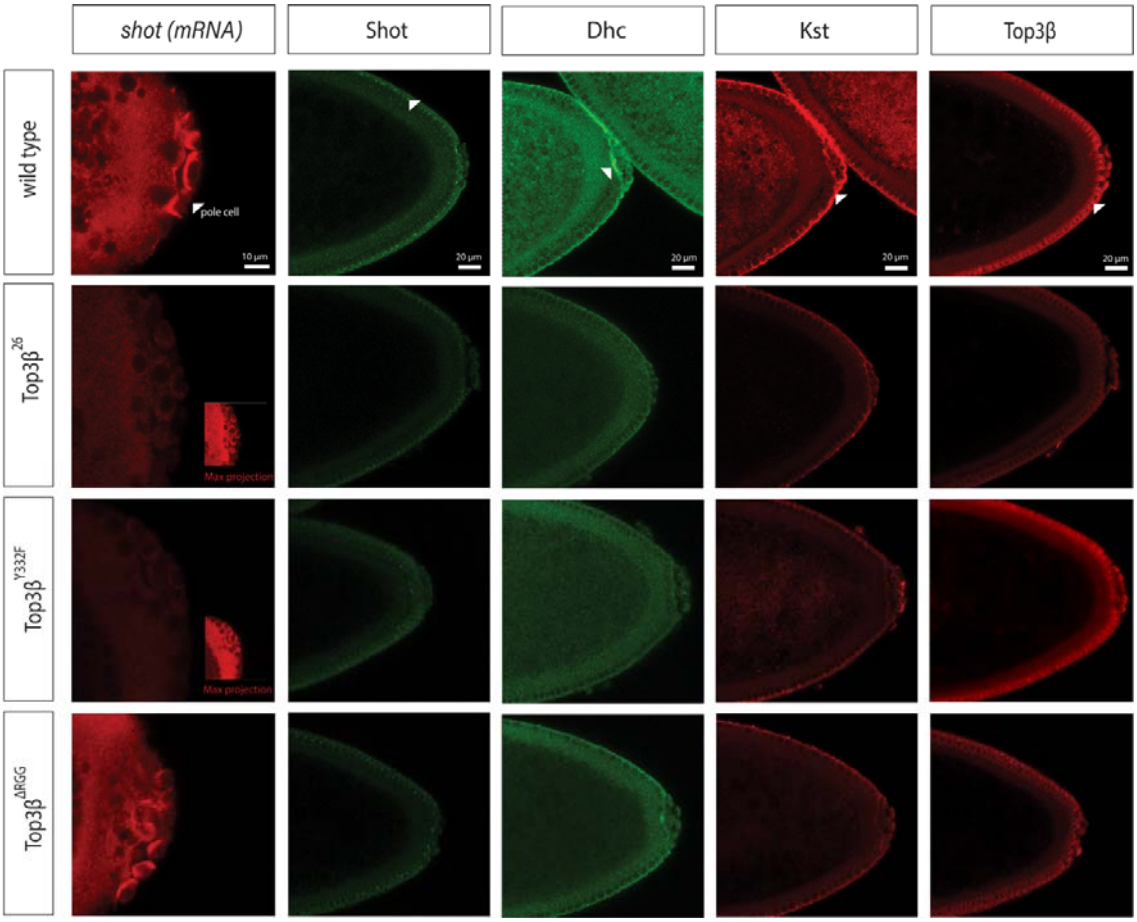

Fig. 5. Expression and localization of gene products of Top3β targets. The posterior pole of the embryos is shown to the right. *shot* mRNA and Shot protein localization in the posterior part of syncytial (*shot* mRNA) and cellularizing (Shot protein) wild-type embryos in the different *Top3β* mutants. Lower signal levels and less localized signals were seen in the null and *Top3β*^{Y332F}. Both were less reduced in *Top3β*$^{\Delta RGG}$ mutant embryos. Note the *shot* mRNA localization in the pole cells in the wild type and *Top3β*$^{\Delta RGG}$ mutant. Dhc64C localization at the posterior side of the somatic part of the embryo (arrowhead) was not detectable in the null mutant and *Top3β*^{Y332F} and reduced in *Top3β*$^{\Delta RGG}$ mutant embryos. Kst localization at the apical membrane (arrowhead) was reduced in null mutants and *Top3β*^{Y332F} compared to the wild type. Its localization was still identifiable in *Top3β*$^{\Delta RGG}$ mutant embryos. Top3β protein is localized similarly to its targets. It is, however absent from the null mutant which reveals the background level of the staining. Note also that Top3β is also nuclear in the wild type and *Top3β*^{Y332F}. Imaging settings were identical for the staining for the same protein and mRNA, respectively, in the different genotypes except for the insets which were overexposed to reveal the embryo. The scale bar is 10µm for the shot mRNA pictures and 20µm for the other micrographs.

Top3β normally localizes to the same area in blastoderm embryos as the different proteins and mRNAs described here. In the Discussion section, we will detail how this seems to contribute to an interesting gene expression mechanism. Note also that the wild-type protein and Top3β^{Y332F} localize to the cytoplasm and the nuclei **(Fig 5)**. In contrast, Top3β$^{\Delta RGG}$ is clearly seen above background levels only in the cytoplasm. This indicates that

356 its RGG box is needed to localize Top3β to the nucleus and that the lack of the RGG box
357 likely reduces the nuclear functions of Top3β$^{\Delta RGG}$.

358 ***Deteriorating neuromuscular structure and function in adult Top3β mutants***

359 The negative geotaxis assay measures the activity of the nervous system and the
360 musculature, and the coordination between them. In this assay, all four genotypes showed
361 similar climbing abilities in young flies **(Fig. 6A).** Neuromuscular conditions sometimes
362 become only apparent at an older age because the young nervous system can compensate
363 for some cellular deficits. But such compensations can take their toll if they stress the cells.
364 We, therefore, tested for premature aging and age-related degeneration of the climbing
365 ability. Indeed, as seen in **Fig. 6A,** from week 6 on, the *Top3β*^{Y332F} and *Top3β*^{26} flies became
366 slower, and their climbing ability declined more than the wild-type one. The results suggest
367 that Top3β plays a crucial role in aging and combating neurodegeneration in *Drosophila*
368 motor neurons.

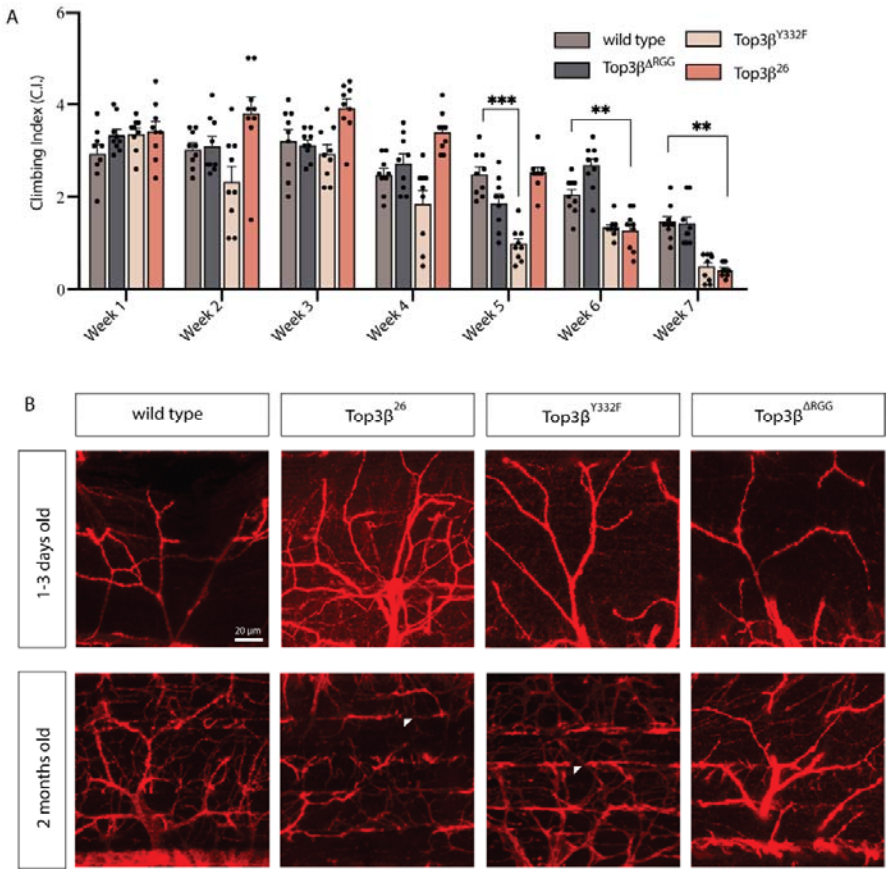

369

Fig. 6: **Aging effects of *Top3β* mutants. A)** Climbing assays of wild type, *Top3β*$^{\Delta RGG}$, *Top3β*^{Y332F}, and *Top3β*^{26} flies. A two-way ANOVA analysis was performed. The graph bars show the mean climbing index (C.I.) for the different genotypes. Error bars represent the standard error of the mean (S.E.M). Each dot represents a calculated individual C.I. The adjusted p-values for each significant difference are indicated on the graph. (p-value <0.0001=****, p-value <0.001=***, p-value <0.01=**, p-value <0.05=*.) **B)** In adults, null mutant NMJs contain more branches than the wild type, indicative of a compensatory mechanism. Arrowheads point to the lost synaptic integrity of dorsal longitudinal flight muscle (DLM). NMJ synapses were visualized by staining of motor neurons with anti-HRP antibodies. The progressive denervation of the DLM is particularly evident in the null and the *Y332F* mutant in the adult thoracic NMJs. The scale bar represents 20µm. All panels show maximum intensity projections with a z-step size of 0.7µm.

As the flies age, their motor abilities and neurotransmission decline, and fragmentation of synaptic motor terminals becomes apparent (24). To gain insights into the possible adaptation of the adult neuromuscular system, we also studied the structure of the adult NMJs in the four genotypes during aging **(Fig. 6B)**. The young null mutants (followed by *Top3β*^{Y332F} and *Top3β*$^{\Delta RGG}$) had more branched structures compared to the simpler branch structures in the wild type. The overgrowth might have arisen to compensate for suboptimal synaptic physiology. However, as the flies age, progressive denervation of the DLM (Dorsal Longitudinal Muscles) synapses in the null mutant occurred, leading to a progressive loss of locomotive ability and more rapid aging **(Fig. 6B).** In both the null and *Top3β*^{Y332F}, a loss of synaptic integrity was observed during aging in 1-2 months old adult flies **(Fig. 6B)**. Because *Top3β*^{26} and *Top3β*^{Y332F} flies live less long than wild-type and *Top3β*$^{\Delta RGG}$ flies **(Supplementary Fig. S3)**, the decline of their NMJ structure and function is most likely even stronger than observed in the living animals. Furthermore, because of the similarity between the phenotypes of *Top3β*^{26} and the *Top3β*^{Y332F} flies, the effect on longevity and aging seems to be caused primarily due to the loss of the enzymatic activity of Top3β, which leads to loss of synaptic integrity, faster aging, and shortened lifespan.

Top3β mutants enhance (G4C2)$_{49}$-induced neuronal toxicity in flies

To gain deeper insights into the cellular significance of Top3β's catalytic activity, we investigated its effect on the phenotype induced by GC-rich repeat RNA sequences. For this, we used the repeat sequence (GGGGCC)$_{49}$ (also named G4C2)$_{49}$ that induces neurotoxic effects in both humans and flies. In humans, the presence of 20-28 repeats of this sequence

405 was shown to be associated with neurodegenerative diseases such as frontotemporal
406 dementia (FTD) and amyotrophic lateral sclerosis (ALS) (25)(26). The accumulation of both
407 sense and antisense repeat strands of this sequence leads to the formation of RNA foci
408 throughout the nervous system, which is believed to be toxic (27). In a fly model for this
409 disease, neuronal cells were engineered to express an RNA with 49 repeats, denoted as
410 $(G4C2)_{49}$, using a Gmr-GAL4 driver (28). Studying the effect of this RNA in the eyes of adult
411 flies revealed that *Top3β* mutants enhanced the neurotoxic effect of the $(G4C2)_{49}$ transcripts
412 in the eyes of young flies aged 1-2 days (**Fig. 7A**). Of the *Top3β* mutants, $Top3\beta^{26}$ and
413 $Top3\beta^{Y332F}$ exhibited the most severe eye lesions with irregular ommatidial structures, and
414 this was particularly evident from the widespread cell death. Young $Top3\beta^{\Delta RGG}$ mutants
415 displayed irregular ommatidia but usually less cell death. After one month, the rough eye
416 phenotype caused by the $Top3\beta^{26}$ and $Top3\beta^{Y332F}$ mutants affected the entire eye, indicating
417 widespread degeneration of ommatidial cells. These results show that the topoisomerase
418 activity of Top3β counteracts the toxic activity of the $(G4C2)_{49}$ transcripts.

419 $(G4C2)_n$ RNAs undergo repeat-associated non-AUG translation, resulting in the production
420 of the dipeptide repeats GA, GP, or GR. There is good evidence that at least some of these
421 repeats can form neurotoxic aggregates (27). To test the involvement of Top3β in the
422 translatability of the $(G4C2)_n$ RNAs in the open reading frame that leads to Glycine-Arginine
423 (GR) repeats, we examined the effect of a transcript containing 44 repeats fused to the open
424 reading frame of the green fluorescent protein (GFP) (UAS-LDS-$(G4C2)^{44GR\text{-}GFP}$; LDS indicates
425 an intronic leader sequence without AUG). By expressing a GR dipeptide under UAS control
426 with the Gmr-GAL4 driver, the GFP tag in the GR reading frame enables fluorescence
427 imaging and quantitation of GR repeat levels in eyes (**Fig. 6B**). The absence of *Top3β* led to
428 the most severe eye lesions but significantly lower levels of GFP signal, implying that fewer
429 GR dipeptides were present. Similar results were observed for $Top3\beta^{Y332F}$. Despite producing
430 milder eye lesions, $Top3\beta^{\Delta RGG}$ mutants still led to reduced GFP signal, indicative of lower
431 levels of GR dipeptides. We conclude that *Top3β* contributes to the production of GR
432 dipeptides. Furthermore, the combined findings suggest that the GR repeats produced in
433 this assay are less responsible for the neurodegeneration of the ommatidial cells. The
434 $(G4C2)_{44}$ RNA itself or one of the other dipeptide repeats are more likely to be the
435 neurotoxic substances.

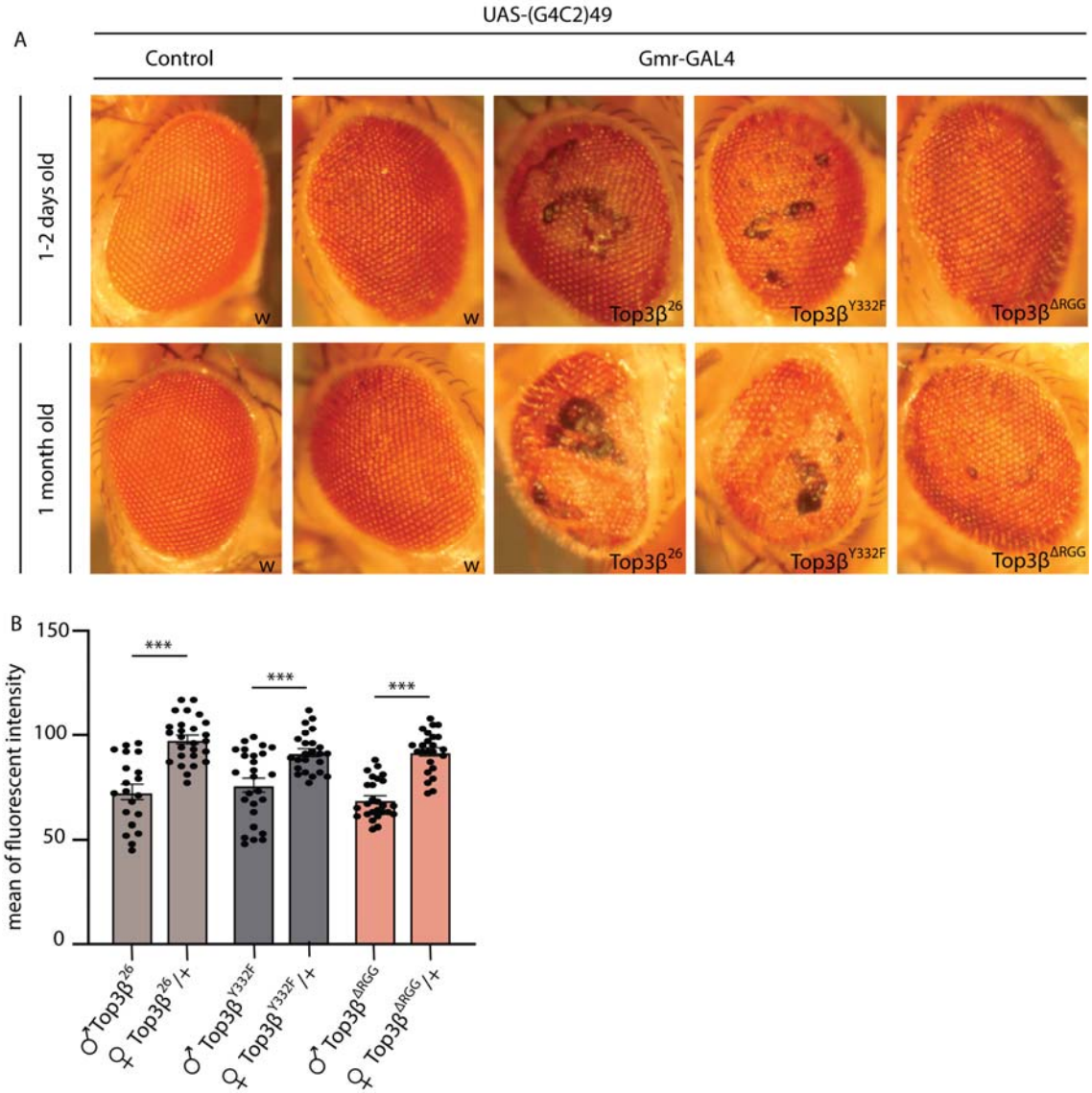

Fig. 7: *Top3β* activities toward $(G4C2)_n$ repeat RNAs in the eye. A) Expression of the UAS-$(G4C2)_{49}$ transgene in wild-type (w) and *Top3β* mutant flies using the Gmr-Gal4 driver. *Top3β*$^{\Delta RGG}$ caused mild disruptions, the *Top3β*^{26} and *Top3β*^{Y332F} mutants caused strong degeneration. Shown are data from one experiment carried out in parallel; data were reproduced in a total of three or more independent experiments. All *Top3β* mutants enhanced the degenerative phenotype of the $(G4C2)_{49}$ RNA. Genotype: *Top3β*^{26} (or *Top3β*^{Y332F} or *Top3β*$^{\Delta RGG}$);;UAS-$(G4C2)_{49}$/GMR-Gal4. GMR-Gal4 control genotype: *w Top3β*$^{+}$; ;UAS-$(G4C2)_{49}$/GMR-Gal4. **B)** *Top3β* mutants reduced the GR-GFP signal in UAS-LDS-$(G4C2)_{44}^{GR\text{-}GFP}$ animals. Quantification of mean GFP fluorescence intensity. Each data point represents the fluorescence of one eye of one animal. Shown are data from one experiment, but data were reproduced in two additional, independent experiments. Male genotype: *Top3β*^{26}*/Y* (or *Top3β*^{Y332F} or *Top3β*$^{\Delta RGG}$); UAS-LDS $(G4C2)_{44}^{GR\text{-}GFP}$/GMR-Gal4, female genotypes (wild-type controls): *Top3β*^{26} (or *Top3β*^{Y332F} /*Top3β*$^{\Delta RGG}$)/+;; UAS-LDS $(G4C2)_{44}^{GR\text{-}GFP}$/GMR-Gal4

450 **Discussion**

451 Top3β and its catalytic activity have an important role in the production of normal
452 expression levels of a considerable number of RNAs during embryonic development. The
453 fact that particularly long pre-mRNAs and RNAs with long open reading frames and long
454 UTRs depend on *Top3β* for their normal expression levels (**Fig. 1**) is consistent with the
455 hypothesis that these long molecules are more dependent on an RNA topoisomerase that
456 can counteract structural problems.

457 The UTRs of mRNA molecules play crucial roles in regulating gene expression through RNA
458 localization and translational control. The dependence on *Top3β* of transcript levels of
459 mRNAs with long 3'UTRs seems to reflect at least in part that these mRNAs need to be
460 transported to particular cellular locations and that they are under translational control
461 (29). These processes are important in large cells like the nervous system, but also for fine-
462 tuning gene expression in general. It is, therefore, not surprising that *Top3β* mutations have
463 been implicated in many neurological diseases and cancers. The (pre)mRNAs that depend on
464 *Top3β* for normal expression in Drosophila embryos <u>and</u> whose homologs have been
465 implicated in one of the neuronal diseases or cancers are particularly long. We see this as
466 evidence in support of the view that large RNAs depend more strongly on *Top3β* and very
467 likely because their length, transport, and translational control provide a strong risk for the
468 inactivation of the RNA due to structural problems. In the context of neural physiology, this
469 finding suggests that Top3β may be important for the timely and local expression of
470 proteins involved in neural development, axonal growth, synaptic physiology, and plasticity.

471 The normal expression levels of the *Ras opposite* (*Rop)* mRNA in young Drosophila embryos
472 depend on *Top3β.* In the context of human neurological diseases this was particularly
473 striking because the human homolog of *Rop* is differentially expressed in <u>all</u> neurological
474 diseases with which human *Top3β* has been associated **(Fig. 2C)**. *Rop* regulates
475 neurotransmitter secretion in a dosage-dependent manner (6) and it had been described to
476 act in synaptic vesicle priming and transport. In *Rop* mutants, the release of
477 neurotransmitters from the pre-synapse area into the synaptic cleft fails to occur. It,
478 therefore, seems that *Rop* could be a rewarding gene to further investigate. ALS and FTD are
479 a subset of neurological diseases that involve GC-rich sequence repeats. In the Drosophila
480 model for this disease, we found that the enzymatic activity of Top3β counteracts the

481 neurodegeneration caused by these GC-rich RNAs (Fig. 7). From what is known about
482 topoisomerases, it appears that Top3β could be doing this by making these RNAs accessible
483 to the cellular pathways that act on it, including translation and degradation.

484 ***RNA targets of Top3β***

485 Finding that Top3β interacts with splicing factors **(Fig. 4)** appears to be a significant result
486 because Top3β's RNA targets have a greater number of exons, longer introns, and
487 alternative transcripts **(Fig. 3)**. The fact that these parameters correlate with one another
488 (30)(31)(32)(33)(34) further strengthens the conclusion that Top3β participates in the
489 nuclear activity of RNA splicing. Moreover, snoRNAs are also enriched in the Top3β targets
490 and recent studies showed that snoRNAs play an important role in the regulation of mRNA
491 splicing and editing and they are also involved in stress response and metabolic homeostasis
492 (35), two additional characteristics of Top3β targets. Even though it would have been
493 interesting to further explore this connection, we focused the presented research on other
494 aspects of *Top3β* activities that seem to relate more to its cytoplasmic functions.

495 Longer pre-mRNAs pose not only more chances for splicing errors (because of the increased
496 difficulty in identifying the correct splice sites) but also for entanglement of the RNA. The
497 latter is also a considerable problem during transport over extended distances, which might
498 even involve mRNA packaging and unpackaging before the mRNAs can be activated for
499 translation at the right place and at the right time. During such transport, extended
500 molecules, such as mRNAs, are likely to become entangled or suffer other structural
501 problems that might interfere with their transport or translation. The coding sequence (CDS)
502 and untranslated regions (UTRs) of an mRNA molecule are also important for regulating
503 gene expression at the level of RNA localization and translation. Particularly 3'UTRs affect
504 not only the translation in neurons but also the localization to the places where these
505 mRNAs will be translated in response to extrinsic stimuli, such as neurotrophins, synaptic
506 activation, and regeneration after injury (36)(8)(37)(38). Consistent with the proposed
507 function of Top3β in rescuing (pre-)mRNAs with the described characteristics, the
508 embryonic targets of Top3β displayed a strong bias for these characteristics (**Figs. 3**) and the
509 enzymatic activity of *Top3β* is particularly important for mRNAs that are generated from
510 long pre-mRNAs, for mRNAs with long 3'UTRs and those with long coding sequences (**Figs.**

511 **1B-D**). These mRNAs are expressed at reduced levels in the absence of the RNA
512 topoisomerase activity and mRNAs with these characteristics were found to bind to Top3β.

513 ***Important targets of Top3β***

514 Localization of mRNAs combined with translational control is a mechanism that is most
515 important in large cells (like oocytes and young embryos) and cells with large extensions
516 (like neurons). Many of the identified mRNAs function in these cells and have important
517 roles in neurons because they encode large cytoskeletal and cortical elements (e.g., *kst*, *α-*
518 *spec*, *shot, mgl*) or regulators of NMJ growth (e.g., *Prosap*). An interesting Top3β target is
519 the *shot* mRNA, which had been identified as a Top3**β** target in Drosophila and mammals,
520 and also as an FMR1 target in mammalian cells (**Fig 3F**; (1)(74)). In Drosophila, normal *shot*
521 mRNA levels also depend on *Top3β* and its enzymatic activity (**Suppl. Table S4**). *shot*
522 encodes a spectraplakin family member, a large cytoskeletal linker molecule that binds actin
523 and microtubules and participates in axon growth and neuromuscular junction maintenance
524 and growth control (39),(40),(41),(42). Drosophila *shot* has additional roles in many other
525 tissues and cell types and it consists of 45 exons producing 22 transcript isoforms, which is
526 many more than the average of 2 isoforms per *Drosophila* gene. *shot* RNA and protein
527 expression in embryos are markedly reduced and less localized in *Top3β* null mutants and in
528 the enzymatically dead $Top3\beta^{Y332F}$ embryos (**Fig. 5**). The enzymatic activity of Top3β is
529 therefore key to the proper expression of *shot* mRNA and protein. The reduced mRNA levels
530 and their failure to localize to specific compartments as they do in the wild type, are
531 consistent with an involvement of Top3β in splicing *shot* pre-mRNAs and in localizing the
532 mRNA, possibly through its activity in resolving RNA entanglements.

533 Along with α-Spec, Kst (β_H-Spectrin) crosslinks F-actin and acts as a molecular scaffold (43)
534 when it is recruited to the apical membrane of epithelial cells (44). The mRNAs encoding
535 these two proteins are both targets of Top3β, and we showed that the normal expression
536 levels and localization of the Kst protein in the embryos depend on the enzymatic activity of
537 Top3β, suggesting that the lack of Top3β affects Kst protein production at the level of *kst*
538 mRNA production, localization and/or translation. Interestingly, Top3β accumulates also
539 preferentially at the apical cortex of embryos, further suggesting that higher Top3β activity
540 in this location may contribute to the apical translatability of apical transcripts – for instance

541 by rescuing entangled mRNAs -, thereby expressing the encoded protein in this location at
542 higher levels, even if the mRNA is uniformly expressed. It thus appears that subcellular
543 localization of Top3β activity might even serve as a novel tool to target gene expression to
544 specific cellular locations even if their mRNAs are expressed uniformly.

545 Finally, we investigated Dhc, the large heavy chain subunit of the cytoplasmic dynein motor
546 complex (75). Being the major retrograde cytoplasmic motor in all cells, neuronal
547 cytoplasmic dynein moves cargo from the synapse along the axon and back to the cell body
548 (45). During Drosophila oogenesis, dynein transports mRNAs, proteins, and organelles from
549 the nurse cells into the oocyte, where they are deposited for the young embryo. In the
550 embryo, it then transports them to the apical cortex (76)(77). We observed reduced protein
551 expression and lack of Dhc concentration at the apical cortex in both the null and *Top3β*^{Y332F}
552 embryos. Again, *Top3β* and its enzymatic activity are needed to allow proper protein
553 expression and the establishment of the proper polar distribution of Dhc with its apical
554 accumulation. There is good evidence for a physical interaction between Top3β and the
555 dynein motor and that it is important for normal cargo localization (1)(46). Top3β forms a
556 complex with Tdrd3 and FMR1 and the latter was shown to interact with the BicD protein,
557 the subunit of the DDB transport machinery. Furthermore, it even depends on this
558 interaction to be transported normally along microtubules and to accumulate at the proper
559 levels and locations in the nervous system.

560 The analysis of the *Top3β*$^{\Delta RGG}$ phenotype revealed that the RGG motif is needed for the
561 nuclear localization of a good fraction of Top3β in the blastoderm embryo **(Fig. 5)**, a process
562 that might also involve dynein transport. The failure of the Top3β$^{\Delta RGG}$ mutant protein to
563 localize to the embryonic nuclei additionally suggests that reduced nuclear functions of
564 Top3β$^{\Delta RGG}$ might contribute to the *Top3β*$^{\Delta RGG}$ mutant phenotype, too.

565 ***Top3β environment and relevance***

566 The enrichment of mRNAs encoding neuronal ribonucleoproteins (RNP) particles, also
567 known as granules, was a clear result of the analysis of our Top3β targets. These RNP
568 granules concentrate specific sets of mRNAs and regulatory proteins in the same location,
569 promoting their common long-distance transport to axons or dendrites (20)(21). They also
570 have a dual function in regulating the translation of associated mRNAs while preventing the

translation of others (47). As a component of neuronal RNPs, Me31B mediates the transport and controls the translation of neuronal RNAs, including the translational repression of synaptic transcripts (26). We found Me31B highly enriched with Top3β and this interaction depended on the RGG box, suggesting that the RGG box links Top3β to the neuronal RNPs.

Consistent with our analysis of physically interacting proteins (**Fig. 4B**), Top3β had already been described to be present in complexes with FMR1 (1). Comparing the datasets of significantly less abundant transcripts in the extracts of *Top3β* mutants (**Supplementary Table S1**) to the data of significantly less translated transcripts upon *Fmr1* RNAi treatment in Drosophila ovaries (48) revealed many shared mRNAs (**Fig. 8)**. Even though different tissues have been used for the two experiments, a large fraction of the ovarian transcripts end up in the young embryo. The overlap between the two data sets indicates that FMR1 and Top3β proteins act on many of the same mRNAs, but that *FMR1* and *Top3β* are also involved in additional functions independently of each other.

A

shared targets in Fmr1 and downregulated RNAs in embryo			
PCB	spir	shi	spri
svr	Atpalpha	Mrtf	Hsc70-3
spen	CG10960	mld	CG31729
oys	toc	Exn	Ack-like
Abl	raskol	Ptp99A	BicD
Glut1	Med	Pde11	Nost
CG43783	Dys	fs(1)h	ctrip
slif	Crag	CG2747	CG13917
Mbs	mtd	stx	SP1029
cnc	CG2818	cana	

B

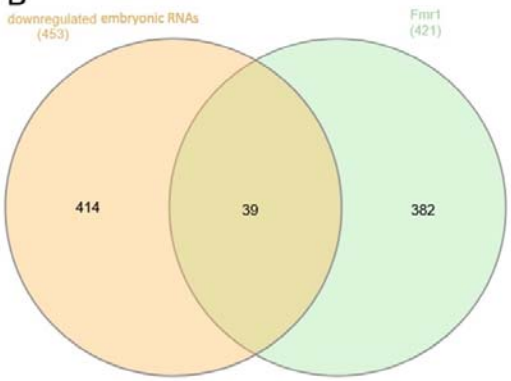

Fig. 8. Ovarian mRNAs depending on *FMR1* for their translation and on *Top3β* for their normal accumulation in young embryos. **A)** List of the shared mRNAs and **B)** Venn diagram of the overlap between the two datasets.

The lack of RNA topoisomerase activity can interfere with the expression of many different genes in a variety of different pathways. The resulting suboptimal functioning of different cellular mechanisms is likely to interfere with cellular physiology, making it less efficient and producing cellular stress. Further research needs to test, which of the individual pathways suggested by our work causes a physiological problem in the human conditions involving *Top3β*. However, serious neurological health issues often arise when several pathways are

596 not functioning properly anymore, making it difficult and possibly less meaningful to
597 pinpoint a primary cause. Our work revealed that reduced activity of Top3β affects several
598 of the pathways that rely on mRNAs that were Top3β targets. The combination of defects in
599 different physiological pathways is likely to impact the outcome of the various
600 neurodevelopmental and cognitive disorders and cancers *Top3β* has been implicated.

601

602 ## Material and Methods

603 ### Fly stocks and maintenance

604 The *white* (*w)* strain was used as a wild-type control as this was the genetic background of
605 the mutants used in this study. The mutant fly stocks *Top3β*^{Y332F} and *Top3β*$^{\Delta RGG}$ were
606 established as described below. *Top3β*^{26} was from Lee and colleagues (49). The fly stocks
607 were grown and maintained on a regular corn medium (ingredients: corn, yeast powder,
608 sucrose syrup, agar, potassium sodium tartrate tetrahydrate, water, nipagin, and propionic
609 acid) supplied with brewer's yeast for the experiments. All *Drosophila melanogaster* fly
610 stocks were stored at 18°C in glass or plastic vials with day/night (12 h/12 h) light cycles. All
611 experiments were performed at 25°C. $(G4C2)_{49}$ flies (Stock #84727) express 49 pure
612 5'GGGGCC3' repeats under the control of UAS and poly(GP)-GFP flies (#84723) 114
613 nucleotides of intronic sequence from the human *C9orf72* gene followed by an expanded
614 G4C2 array of 44 (or fewer repeats according to the note in the stock description). The G4C2
615 arrays can produce three dipeptides, GA, GR, and GP, with the GR dipeptide open reading
616 frame being GFP-tagged at the 3' end for use in this study (78). These repeats are neurotoxic
617 and model the G4C2 repeats seen in human *C9orf72* that are associated with Amyotrophic
618 Lateral Sclerosis and Frontotemporal Dementia.

619

620 ### Generation of *Top3β* alleles

621 Genomic sequences were scanned for suitable sgRNA target sites with the JBrowse from
622 FlyBase and appropriate sgRNA sequences were chosen based on (a) their distance from the
623 tagging site, and (b) the absence of potential off-target sites on the same chromosome as
624 the target site (51). To mutate the endogenous *Top3β*, a sgRNA was designed, which
625 hybridized in the vicinity of the Y332 codon of *Top3β* and induced the Cas9 nuclease to
626 perform a double-strand break. Complementary oligodeoxynucleotides with suitable
627 overhangs (**Supplementary Table S6**) were annealed and cloned into the pCFD5 vector,
628 which is used to express the sgRNA (52). The Cas9 fly stock was obtained from the
629 Bloomington Stock Center (#79004). ssDNA was designed for the mutation changing the Tyr
630 (Y) to a Phe (F) codon and injected into the progeny produced by Cas9- and sgRNA-
631 expressing flies. The single-strand oligodeoxynucleotide with the flanking arms precisely

632 matching the endogenous sequences changes the sequence at the mutation site by serving
633 as a template (**Supplementary Table S6**) for the homologous recombination DNA repair at
634 the double-strand break. The same strategy was used to delete the endogenous RGG region
635 in *Top3β* (ΔRGG) using the appropriate gRNA and ssDNA templates.

636

637 **RNA sequencing**

638 RNA sequencing was performed using 1 mL of TRIzol® Reagent per 50-100 mg of tissue
639 samples (0-2 hours embryos and 1-5 days old heads), which were homogenized at room
640 temperature. RNA extraction was done according to the Trizol protocol. The University of
641 Bern's Next Generation Sequencing Platform conducted quality control assessments, library
642 generation, sequencing runs, and sequencing quality control steps. The purified total RNA
643 was assessed for quantity and quality using a Thermo Fisher Scientific Qubit 4.0 fluorometer
644 with the Qubit RNA BR or HS Assay Kit (Thermo Fisher Scientific, Q10211 or Q32855,
645 respectively) and an Agilent Advanced Analytical Fragment Analyzer System using a
646 Fragment Analyzer RNA Kit (Agilent, DNF-471), respectively. Sequencing libraries were made
647 using a CORALL Total RNA-Seq Library Prep Kit with UDI 12nt Set A1 (Lexogen, 117.96)
648 according to Lexogen's guidelines. The libraries were paired-end sequenced using either
649 shared Illumina NovaSeq 6000 SP, S1, or S2 Reagent Kits (200 cycles; Illumina, 200240719,
650 2002831, or 20028315) on an Illumina NovaSeq 6000 instrument. The quality of the
651 sequencing runs was assessed using the Illumina Sequencing Analysis Viewer (Illumina
652 version 2.4.7), and all base call files were demultiplexed and converted into FASTQ files
653 using Illumina bcl2fastq conversion software v2.20.

654 The quality and quantity of reads generated from RNA-seq were evaluated. Most of the
655 reads were from mature transcripts without introns, but we mapped them to the reference
656 genome that includes introns using an alignment tool like Hisat2 that can handle large gaps.
657 This required information on where each gene is located in the genome, available for
658 example from Ensemble (53). The number of reads mapping to each gene was counted
659 using the FeatureCounts tool, which requires information about the location of each gene in
660 the genome. This resulted in a table of read counts for each sample and gene.

661 To test for differential expression between two experimental groups containing three
662 biological replicates each, we used the DESeq2 tool. The analysis included the following
663 steps: 1. Normalization to correct for differences in the total number of reads between
664 samples. 2. Variance estimation between replicates to account for the limited number of
665 replicates in RNA-seq experiments (DESeq2 incorporates information from other genes with
666 similar overall expression levels into the estimation). 3. Log-fold change (LFC) adjustment
667 based on evidence strength which was estimated by the LFC. If it is weak (e.g., because the
668 gene is expressed at low levels, the variance between replicates is high, or there are few
669 replicates), the LFC shrinks toward zero. 4. Calculation of a test statistic and comparison to
670 the normal distribution to obtain a p-value. 5. Multiple test corrections using the Benjamini-
671 Hochberg procedure to consider only potentially detectable, differentially expressed genes.
672 DESeq2 applies a false discovery rate correction based on the Benjamini-Hochberg
673 procedure. However, the multiple-test correction considers only genes that could
674 potentially be detected as differentially expressed. Only these genes will have an adjusted p-
675 value. The mean read count across all samples is used to decide if a gene should be included
676 or not.

677

678 **Extracting transcript features**

679 The information about exon length, exon count, 3´UTR length, gene name, gene length,
680 5´UTR length, mRNA length, and CDS length was extracted from the gtf file of dmel-all-
681 filtered-r6.42.gff using a custom python script.

682

683 **Generation of the *Top3β::eGFP* cDNA clone for GAL4>UAS expression**

684 For the *Top3β::eGFP* construct, the *Top3β* cDNA clone LD10035 was amplified. Enhanced
685 GFP (EGFP) was PCR amplified from a plasmid (pEGFP–C3). PCR amplified fragments were
686 run on an agarose gel and purified using the Wizard SV kit (Promega). The sequences were
687 cloned into the pUASz1.0 vector (54) with the *eGFP* ORF at the C-terminal end of the *Top3β*
688 ORF using a ligation kit (NEB). The UASz vector allows one to induce the constructs in any
689 tissue, including the somatic tissue, the germline, and the CNS (54). Plasmids were
690 sequenced to confirm the integrity of the construct and purified with a PureYield kit

691 (Promega) for injection. Transgenic stocks were established with the attP landing platform
692 86F from the Bloomington Stock Center (#24749).

693 To generate an enzymatically dead enzyme, a Phe codon substituted the codon for the Tyr
694 responsible for crosslinking the enzyme with the nucleic acid in the *UASz-Top3β::eGFP*
695 vector to give rise to *UASz-Top3β*^{Y332F}*::eGFP*. Similarly, to figure out the role of the RGG box,
696 we deleted in the in the *UASz-Top3β::eGFP* vector the sequence coding for this box, giving
697 rise to *UASz-Top3β*$^{\Delta RGG}$*::eGFP*. At the site of the desired mutation, oligonucleotide primers
698 with the desired mutation were used to amplify the mutant double-stranded DNA plasmid
699 (**Supplementary Table S6)**. A protocol based on two different PCR amplifications was used
700 for this. First, two elongation reactions were carried out, with one of the two primers each.
701 In the second reaction, the two initial elongation reactions were mixed and an additional
702 PCR reaction was carried out. The wild-type and mutant eGFP fusion constructs were
703 transformed into *Drosophila* using the attP-86F landing platform. mat-tub-Gal4 (#7062) was
704 used to drive the expression in the older female germline and Gal4-BG380 (#24749) to drive
705 expression in the CNS. UASz-eGFP transgenic flies, obtained from the Bloomington stock
706 center, were used as negative controls.

707

708 **Sample preparation for mass spectrometry**

709 Drosophila Top3β::eGFP was purified using the GFP tag and a mouse anti-eGFP antibody as
710 described previously (55). Protein G magnetic beads were washed 3x with PBS and
711 incubated for 2 hours with an anti-GFP antibody. After this, they were washed 3x with 1 ml
712 1x PBS and one more time with 1 ml homogenization buffer (25 mM Hepes PH 7.4; 150 mM
713 NaCl; 0.5 mM EDTA PH 8.0, 1 mM DTT, protease inhibitors). To prepare the extracts, 1 ml
714 homogenization buffer was added to 1 gr of the samples (dechorionated embryos 0-2 hours
715 or adult heads 1-5 days old) in the glass homogenizer. The samples were homogenized and
716 transferred into the tube. Homogenized samples were centrifuged at 16,000 g (RCF), 4°C for
717 40 min. The interphase was transferred into a fresh Eppendorf tube, centrifuged again at
718 16,000 g, 4°C for 40 min, and transferred into a fresh tube. Beads were then incubated with
719 the extracts for 6 hours at 4°C on a wheel and the extracts were subsequently removed
720 from the beads. The beads were washed once with 1 ml homogenization buffer and then

721 several times with wash buffer (25 mM Hepes PH 7.4; 150 mM NaCl; 0.5 mM EDTA PH 8.0; 1
722 mM DTT; protease inhibitors). The wash buffer was removed, and the beads were sent for
723 mass spectrometry.

724

725 **Mass spectrometry**

726 Mass spectrometry analysis was done by the Proteomics and Mass Spectrometry Core
727 Facility of the University of Bern, and the data are available in **Supplementary Table S5**.
728 Proteins in the affinity pull-down were re-suspended in 8M Urea / 50 mM Tris-HCl pH8,
729 reduced for 30 min at 37°C with 0.1M DTT / 100 mM Tris-HCl pH8, alkylated for 30 min at
730 37°C in the dark with IAA 0.5M / 100 mM Tris-HCl pH8, dilute with 4 volumes of 20 mM Tris-
731 HCl pH8 / 2 mM CaCl2 before overnight digestion at room temperature with 100 ng
732 sequencing grade trypsin (Promega). Samples were centrifuged, and a magnet holder
733 trapped the magnetic beads to extract the peptides in the supernatant. The digests were
734 analyzed by liquid chromatography (LC)-MS/MS (PROXEON coupled to a QExactive mass
735 spectrometer, ThermoFisher Scientific) with three injections of 5 µl digests. Peptides were
736 trapped on a µPrecolumn C18 PepMap100 (5 µm, 100 Å, 300 µm×5 mm, ThermoFisher
737 Scientific, Reinach, Switzerland) and separated by backflush on a C18 column (5 µm, 100 Å,
738 75 µm×15 cm, C18) by applying a 60 min gradient of 5% acetonitrile to 40% in water, 0.1%
739 formic acid, at a flow rate of 350 ml/min. The Full Scan method was set with a resolution at
740 70,000 with an automatic gain control (AGC) target of 1E06 and a maximum ion injection
741 time of 50 ms. The data-dependent method for precursor ion fragmentation was applied
742 with the following settings: resolution 17,500, AGC of 1E05, maximum ion time of 110
743 milliseconds, mass window 2 m/z, collision energy 27, underfill ratio 1%, charge exclusion of
744 unassigned and 1+ ions, and peptide match preferred, respectively.

745 The data were then processed with the software MaxQuant (56) version 1.6.14.0 against the
746 UniProtKB(57) Drosophila 7228 database (release 2021_02) containing canonical and
747 isoform entries, to which common contaminants were added. The following parameters
748 were set: digestion by strict trypsin (maximum three missed cleavages), first search peptide
749 tolerance of 15 ppm, MS/MS match tolerance of 20 ppm, PSM and protein FDR set to 0.01
750 and a minimum of 2 peptides requested per group. Carbamidomethylation on cysteine was

751 selected as a fixed modification; the following variable modifications were allowed:
752 methionine oxidation, deamidation of asparagines and glutamines, and protein N-terminal
753 acetylation; a maximum of 3 modifications per peptide was allowed. Match between runs
754 was turned on (match time windows 0.7 min) but only allowed within replicates of the same
755 kind.

756 Peptides were normalized by variance stabilization (58), imputed and combined to form
757 Top3 (59) intensities, and considered alongside MaxQuant's Label-Free Quantification (LFQ)
758 values. Missing peptides, respectively LFQ intensities, were imputed by drawing values from
759 a Gaussian distribution of width 0.3 centered at the sample distribution mean minus 2.5x
760 the sample standard deviation, provided there were at most 1 non zero value in the group;
761 otherwise, the Maximum Likelihood Estimation (60) was used. Differential expression was
762 performed by applying the empirical Bayes test (61) between groups; significance testing
763 was performed as described (62).

764

765 **RNA immunoprecipitation**

766 Protein G magnetic beads were washed 2-3x with 1ml blocking buffer (20 mM Hepes, 150
767 mM KCl, 20% Glycerol, 0.5 % Tween, BSA (Biolabs), Heparin 0.2 mg/ml, SDS 0.1%, 1/2 pill
768 EDTA free protease inhibitors). Beads were blocked with a blocking buffer for 2-3 hours at
769 room temperature. An anti-GFP antibody was added to the beads and rotated for 1-2 hours.
770 Beads were washed 3x with non-hypotonic lysis buffer (20 mM Hepes, 1 mM EDTA, 150 mM
771 KCL, 1 mM DTT, 0.5% Tween, 20% glycerol, SDS 0.1%, 1/2 pill EDTA free protease inhibitors).
772 Anti-GFP antibody was added to the beads and rotated for 1-2 hours at room temperature.
773 Beads were washed 3x with non-hypotonic lysis buffer.

774 Dechorionated embryos were 0-2 hours old. 1g of the embryos were homogenized in 2 ml
775 hypotonic lysis buffer (20 mM Hepes, 10 mM KCL, 1 mM EDTA, 1 mM DTT, 0.5% Tween, SDS
776 0.1%, 1/2 pill EDTA free protease inhibitors, and RNase inhibitor (Biolabs, 40,000U/ml)). 600
777 μl of extract, 323 μl of Adjusting buffer (57% Glycerol 100%, 0.4M KCl, 1 mM EDTA, 1 mM
778 DTT, 20 mM Hepes, SDS 0.1%), and 2 μl of RNase-free DNase I (20 μ/ml, Roche) were added
779 to the washed antibody beads and were precipitated ON rotating at 4°C. Samples were
780 washed 8x with 1 ml high salt wash buffer (20 mM Hepes, 1 mM EDTA, 200 mM KCl, 1 mM

781 DTT, 0.5% Tween, 20% Glycerol, SDS 0.1%, 1/2 pill EDTA free protease inhibitors, and RNase
782 inhibitor (Biolabs, 40,000U/ml)). On the last wash, 100 µl of the samples were taken before
783 centrifugation. 100 µl of proteinase K buffer, 1.5 µl proteinase K (20 mg/ml Roche), and
784 RNase inhibitors were added to each tube and were incubated for 30 minutes at 55°C. 1 ml
785 Trizol reagent was added to each tube, and RNA was extracted according to the Trizol
786 protocol (TRIzol™ Reagent, Invitrogen™, Catalog number: 15596026).

787 The Next Generation Sequencing Platform, University of Bern, conducted quality control
788 assessments, library generation, sequencing runs, and sequencing quality control steps. The
789 quantity and quality of the purified total RNA were assessed using a Thermo Fisher Scientific
790 Qubit 4.0 fluorometer with the Qubit RNA BR or HS Assay Kit (Thermo Fisher Scientific,
791 Q10211 or Q32855, respectively) and an Advanced Analytical Fragment Analyzer System
792 using a Fragment Analyzer RNA Kit (Agilent, DNF-471), respectively. Sequencing libraries
793 were made using a CORALL Total RNA-Seq Library Prep Kit, Version 1 with UDI 12nt Set A1
794 (Lexogen, 117.96) according to Lexogen's guidelines for this kit. Pooled cDNA libraries were
795 paired-end sequenced using either shared Illumina NovaSeq 6000 SP, S1, or S2 Reagent Kits
796 (200 cycles; Illumina, 200240719, 2002831, or 20028315) on an Illumina NovaSeq 6000
797 instrument. The quality of the sequencing run was assessed using Illumina Sequencing
798 Analysis Viewer (Illumina version 2.4.7) and all base call files were demultiplexed and
799 converted into FASTQ files using Illumina bcl2fastq conversion software v2.20.

800 The quality of the RNA-seq reads was assessed using fastqc v0.11.9 (63) and RSeQC v4.0.0
801 (64). Unique molecular identifiers (UMI) were extracted with umi-tools v1.1.2 (65), and
802 adapters were trimmed with cutadapt v3.4.1 (66) according to manufacturer instructions.
803 The reads were aligned to the Drosophila reference genome (BDGP6.32) using hisat2 v2.2.1
804 (67). FeatureCounts v2.0.1 (68) was used to count the number of reads overlapping with
805 each gene as specified in release 103 of the Ensembl genome annotation. The Bioconductor
806 package DESeq2 v1.36.0 (69) was used to test for differential gene expression between the
807 experimental groups. To generate the log2 fold change versus transcript length plots, the
808 estimated log2 fold change per gene was plotted against the most extended transcript
809 length per gene with R v4.2.1 (70). We used the log2 fold change>=1 and the adjusted p-
810 value (adjp-value) <0.05 of enrichment over control for further analysis.

811

812 **Dissection and immunostaining of adult Dorsal Longitudinal Muscles (DLMs)**

813 Thoraces of 0-3 days old and 2 months old adult wild-type, *Top3β*^{Y332F}, *Top3β*$^{\Delta RGG}$, and
814 *Top3β*^{26} flies were separated from the rest of the body in 1x PBS. The thoraces were fixed in
815 PFA (32% formaldehyde diluted to 4% with 1x PBS) for 30 min at room temperature and
816 then washed 3x with PBS. All 1x PBS was removed from the tubes using a Pasteur pipette.
817 The tubes were submerged into a liquid nitrogen flask for 10 seconds using cryogenic
818 tweezers. Then, 300 µL of ice-cold 1x PBS was added to the samples. The thoraxes were cut
819 into two hemithoraxes, transferred into 1x PBS (24), and blocked in 1x PBS with 0.1% normal
820 goat serum and 0.2% Triton X-100 at pH 7.4 for at least one h at 4°C. Mouse anti-HRP or
821 anti-Brp (nc82; 1:125 dilution) from Developmental Studies Hybridoma Bank were used to
822 stain motor neurons. Primary antibodies were removed on the following day and the tissue
823 was washed four times with PBST for 5 min each on a rotator. For the secondary antibody
824 staining, goat anti-mouse A647 (1.5 mg/ml, diluted 1:200 dilution; Jackson ImmunoResearch
825 Laboratories Inc.) was added to the samples, which were then kept at room temperature for
826 2 hours in a dark box on the rotator. After the 2 h incubation, the secondary stain was
827 washed out 4 times for 5 min with PBST. Then, the samples were mounted on a slide (24).

828

829 **Negative geotaxis (climbing) assays**

830 Wild-type flies and the three *Top3β* mutant strains were reared on fresh food and allowed
831 to hatch at 25° C. For each genotype, all 0-3-day-old adult male flies were collected. Ten
832 young adult male flies, each, were anesthetized and placed in 4 separate graduated flat
833 bottom glass cylinders. After 1 hour of recovery from CO_2 exposure, flies were gently tapped
834 4x to the bottom of the cylinder to startle them repeatedly with constant force to displace
835 the flies to the bottom surface. The flies were then allowed to climb the wall until they
836 reached the top of the column. The climbing procedure was video recorded using an iPhone
837 11 Pro. These assays were repeated every week over 7 weeks on the same weekday. Three
838 fly batches, each, provided the material for the triplicates which were performed within 5-
839 minute intervals. After the three trials, each batch of 10 flies was transferred into glass vials
840 and kept at 25° C. Before the experiment, every single batch was inspected to ensure that all

841 40 flies could be video-tracked when they started to climb after the tapping. To calculate
842 each climbing index (CI), flies that remained at the bottom were counted as in zone 0. The
843 formula used to calculate the CI is CI = (0 x n0 + 1 x n1 + 2 x n2 + 3 x n3 + 4 x n4 + 5 x n5) /
844 nTotal, where nTotal is the total number of flies and nx is the number of flies that reached
845 zone x.

846

847 **Statistics**

848 All statistical analyses were performed using GraphPad Prism 8. For the negative geotaxis
849 assays, the means, standard error of the means, and p-values were obtained by two-way
850 ANOVA with Tukey's multiple comparison test.

851

852 **Acknowledgments**

853 Our thanks go to P. Nicholson and the members of the University of Bern NGS platform for
854 sequencing the many RNA samples and to the IBU group of R. Bruggmann, particularly, S.
855 Oberhänsli and G. van Geest, for their important support during the analyses of the
856 sequencing data. We thank the University of Bern (Switzerland) Mass Spectrometry Center
857 (PMSCF) members S. Braga Lagache and N. Buchs for performing the MS experiments and
858 M. Heller and A-C. Uldry for the data analysis. We wish to acknowledge all our group
859 members who gave their time and expertise to provide critical input and technical support.
860 Special thanks go to P. Vazquez, R. Dörig, and D. Beuchle. We highly appreciate the
861 continuous support from friends and colleagues in the fly community for sharing their
862 results, fly stocks, and antibodies. For this work, too, FlyBase provided invaluable support,
863 the Developmental Studies Hybridoma Bank provided antibodies, and the Bloomington
864 Drosophila Stock Center (NIH P40OD018537) fly stocks.

865

866 **Funding**

867 This work was supported by the Swiss National Science Foundation project grants
868 31003A_173188 and 310030_205075 and by the Equipment grant 316030_150824 to BS.
869 Support came also from the University of Bern to BS. The funders had no role in study
870 design, data collection, and interpretation, or the decision to submit the work for
871 publication.

872 **References**

873 1. Xu D, Shen W, Guo R, Xue Y, Peng W, Sima J, et al. Top3β is an RNA topoisomerase
874 that works with fragile X syndrome protein to promote synapse formation. Nat
875 Neurosci. 2013;16(9):1238.

876 2. Ahmad M, Shen W, Li W, Xue Y, Zou S, Xu D, et al. Topoisomerase 3β is the major
877 topoisomerase for mRNAs and linked to neurodevelopment and mental dysfunction.
878 Nucleic Acids Res. 2017;45(5):2704–13.

879 3. Kaufman CS, Genovese A, Butler MG. Deletion of TOP3B is associated with cognitive
880 impairment and facial dysmorphism. Cytogenet Genome Res. 2016;150(2):106–11.

881 4. Dekker NH, Rybenkov V V, Duguet M, Crisona NJ, Cozzarelli NR, Bensimon D, et al.
882 The mechanism of type IA topoisomerases. Proc Natl Acad Sci. 2002;99(19):12126–
883 31.

884 5. Piñero J, Saüch J, Sanz F, Furlong LI. The DisGeNET cytoscape app: Exploring and
885 visualizing disease genomics data. Comput Struct Biotechnol J. 2021;19:2960–7.

886 6. Wu MN, Littleton JT, Bhat MA, Prokop A, Bellen HJ. ROP, the Drosophila Sec1
887 homolog, interacts with syntaxin and regulates neurotransmitter release in a dosage-
888 dependent manner. EMBO J. 1998;17(1):127–39.

889 7. Schulze KL, Littleton JT, Salzberg A, Halachmi N, Stern M, Lev Z, et al. Rop, a
890 Drosophila homolog of yeast Sec1 and vertebrate n-Sect/Munc-18 proteins, is a
891 negative regulator of neurotransmitter release in vivo. Neuron. 1994;13(5):1099–108.

892 8. Zhang W, Liu HT. MAPK signal pathways in the regulation of cell proliferation in
893 mammalian cells. Cell Res. 2002;12(1):9–18.

894 9. Huang R, Quan Y, Chen J, Wang T, Xu M, Ye M, et al. Osteopontin promotes cell
895 migration and invasion, and inhibits apoptosis and autophagy in colorectal cancer by
896 activating the p38 MAPK signaling pathway. Cell Physiol Biochem. 2017;41(5):1851–
897 64.

898 10. Baker NM, Rajan R, Mondragón A. Structural studies of type I topoisomerases.
899 Nucleic Acids Res. 2009;37(3):693–701.

900 11. Pommier Y, Sun Y, Shar-yin NH, Nitiss JL. Roles of eukaryotic topoisomerases in
901 transcription, replication and genomic stability. Nat Rev Mol cell Biol.
902 2016;17(11):703.

903 12. Nostramo R, Xing S, Zhang B, Herman PK. Insights into the role of P-bodies and stress
904 granules in protein quality control. Genetics. 2019;213(1):251–65.

905 13. Siaw GE-L, Liu I-F, Lin P-Y, Been MD, Hsieh T. DNA and RNA topoisomerase activities
906 of Top3β are promoted by mediator protein Tudor domain-containing protein 3. Proc
907 Natl Acad Sci. 2016;113(38):E5544–51.

908 14. Nakamura A, Amikura R, Hanyu K, Kobayashi S. Me31B silences translation of oocyte-
909 localizing RNAs through the formation of cytoplasmic RNP complex during Drosophila
910 oogenesis. 2001;

911 15. Wilhelm JE, Buszczak M, Sayles S. Efficient protein trafficking requires trailer hitch, a

912 component of a ribonucleoprotein complex localized to the ER in Drosophila. Dev
913 Cell. 2005;9(5):675–85.

914 16. Barbee SA, Estes PS, Cziko A-M, Hillebrand J, Luedeman RA, Coller JM, et al. Staufen-
915 and FMRP-containing neuronal RNPs are structurally and functionally related to
916 somatic P bodies. Neuron. 2006;52(6):997–1009.

917 17. Liu J, Carmell MA, Rivas F V, Marsden CG, Thomson JM, Song J-J, et al. Argonaute2 is
918 the catalytic engine of mammalian RNAi. Science (80-). 2004;305(5689):1437–41.

919 18. Wang M, Ly M, Lugowski A, Laver JD, Lipshitz HD, Smibert CA, et al. ME31B globally
920 represses maternal mRNAs by two distinct mechanisms during the Drosophila
921 maternal-to-zygotic transition. Elife. 2017;6:e27891.

922 19. Lee J, Yoo E, Lee H, Park K, Hur J-H, Lim C. LSM12 and ME31B/DDX6 define distinct
923 modes of posttranscriptional regulation by ATAXIN-2 protein complex in Drosophila
924 circadian pacemaker neurons. Mol Cell. 2017;66(1):129–40.

925 20. Hillebrand J, Barbee SA, Ramaswami M. P-body components, microRNA regulation,
926 and synaptic plasticity. ScientificWorldJournal. 2007;7:178–90.

927 21. Ruscica V, Bawankar P, Peter D, Helms S, Igreja C, Izaurralde E. Direct role for the
928 Drosophila GIGYF protein in 4EHP-mediated mRNA repression. Nucleic Acids Res.
929 2019;47(13):7035–48.

930 22. Lee S, Kolodziej PA. Short Stop provides an essential link between F-actin and
931 microtubules during axon extension. 2002;

932 23. Liu Z, Steward R, Luo L. Drosophila Lis1 is required for neuroblast proliferation,
933 dendritic elaboration and axonal transport. Nat Cell Biol. 2000;2(11):776–83.

934 24. Sidisky JM, Babcock DT. Visualizing synaptic degeneration in adult Drosophila in
935 association with neurodegeneration. JoVE (Journal Vis Exp. 2020;(159):e61363.

936 25. DeJesus-Hernandez M, Mackenzie IR, Boeve BF, Boxer AL, Baker M, Rutherford NJ, et
937 al. Expanded GGGGCC hexanucleotide repeat in noncoding region of C9ORF72 causes
938 chromosome 9p-linked FTD and ALS. Neuron. 2011;72(2):245–56.

939 26. Renton AE, Majounie E, Waite A, Simón-Sánchez J, Rollinson S, Gibbs JR, et al. A
940 hexanucleotide repeat expansion in C9ORF72 is the cause of chromosome 9p21-
941 linked ALS-FTD. Neuron. 2011;72(2):257–68.

942 27. Vatsavayai SC, Nana AL, Yokoyama JS, Seeley WW. C9orf72-FTD/ALS pathogenesis:
943 evidence from human neuropathological studies. Acta Neuropathol. 2019;137:1–26.

944 28. Goodman LD, Prudencio M, Kramer NJ, Martinez-Ramirez LF, Srinivasan AR, Lan M, et
945 al. Toxic expanded GGGGCC repeat transcription is mediated by the PAF1 complex in
946 C9orf72-associated FTD. Nat Neurosci. 2019;22(6):863–74.

947 29. Mignone F, Gissi C, Liuni S, Pesole G. Untranslated regions of mRNAs. Genome Biol.
948 2002;3:1–10.

949 30. Ast G. How did alternative splicing evolve? Nat Rev Genet. 2004;5(10):773–82.

950 31. Black DL. Protein diversity from alternative splicing: a challenge for bioinformatics

951 and post-genome biology. Cell. 2000;103(3):367–70.

952 32. Budagyan B, Loraine A. Gene length and alternative transcription in fruit fly. In:
953 Proceedings 2004 IEEE Computational Systems Bioinformatics Conference, 2004 CSB
954 2004. IEEE; 2004. p. 515–6.

955 33. McGuire AM, Pearson MD, Neafsey DE, Galagan JE. Cross-kingdom patterns of
956 alternative splicing and splice recognition. Genome Biol. 2008;9(3):1–19.

957 34. Fox-Walsh KL, Dou Y, Lam BJ, Hung S, Baldi PF, Hertel KJ. The architecture of pre-
958 mRNAs affects mechanisms of splice-site pairing. Proc Natl Acad Sci.
959 2005;102(45):16176–81.

960 35. Liang J, Wen J, Huang Z, Chen X, Zhang B, Chu L. Small nucleolar RNAs: insight into
961 their function in cancer. Front Oncol. 2019;9:587.

962 36. Han K, Gennarino VA, Lee Y, Pang K, Hashimoto-Torii K, Choufani S, et al. Human-
963 specific regulation of MeCP2 levels in fetal brains by microRNA miR-483-5p. Genes
964 Dev. 2013;27(5):485–90.

965 37. Tushev G, Glock C, Heumüller M, Biever A, Jovanovic M, Schuman EM. Alternative 3
966 UTRs modify the localization, regulatory potential, stability, and plasticity of mRNAs in
967 neuronal compartments. Neuron. 2018;98(3):495–511.

968 38. Glock C, Biever A, Tushev G, Nassim-Assir B, Kao A, Bartnik I, et al. The translatome of
969 neuronal cell bodies, dendrites, and axons. Proc Natl Acad Sci. 2021;118(43).

970 39. Dewey EB, Parra AS, Johnston CA. Loss of the spectraplakin gene Short stop induces a
971 DNA damage response in Drosophila epithelia. Sci Rep. 2020;10(1):1–13.

972 40. Sanchez-Soriano N, Travis M, Dajas-Bailador F, Gonçalves-Pimentel C, Whitmarsh AJ,
973 Prokop A. Mouse ACF7 and drosophila short stop modulate filopodia formation and
974 microtubule organisation during neuronal growth. J Cell Sci. 2009;122(14):2534–42.

975 41. Prokop A, Beaven R, Qu Y, Sánchez-Soriano N. Using fly genetics to dissect the
976 cytoskeletal machinery of neurons during axonal growth and maintenance. J Cell Sci.
977 2013;126(11):2331–41.

978 42. Valakh V, Walker LJ, Skeath JB, DiAntonio A. Loss of the spectraplakin short stop
979 activates the DLK injury response pathway in Drosophila. J Neurosci.
980 2013;33(45):17863–73.

981 43. Bennett V, Baines AJ. Spectrin and ankyrin-based pathways: metazoan inventions for
982 integrating cells into tissues. Physiol Rev. 2001;81(3):1353–92.

983 44. Thomas GH, Williams JA. Dynamic rearrangement of the spectrin membrane skeleton
984 during the generation of epithelial polarity in Drosophila. J Cell Sci.
985 1999;112(17):2843–52.

986 45. Banks GT, Fisher E. Cytoplasmic dynein could be key to understanding
987 neurodegeneration. Genome Biol. 2008;9(3):1–4.

988 46. Bianco A, Dienstbier M, Salter HK, Gatto G, Bullock SL. Bicaudal-D regulates fragile X
989 mental retardation protein levels, motility, and function during neuronal
990 morphogenesis. Curr Biol. 2010;20(16):1487–92.

991 47. Formicola N, Vijayakumar J, Besse F. Neuronal ribonucleoprotein granules: Dynamic
992 sensors of localized signals. Traffic. 2019;20(9):639–49.

993 48. Greenblatt EJ, Spradling AC. Fragile X mental retardation 1 gene enhances the
994 translation of large autism-related proteins. Science (80-). 2018;361(6403):709–12.

995 49. Lee SK, Xue Y, Shen W, Zhang Y, Joo Y, Ahmad M, et al. Topoisomerase 3β interacts
996 with RNAi machinery to promote heterochromatin formation and transcriptional
997 silencing in Drosophila. Nat Commun. 2018;9(1):4946.

998 51. Gratz SJ, Rubinstein CD, Harrison MM, Wildonger J, O'Connor-Giles KM. CRISPR-Cas9
999 genome editing in Drosophila. Curr Protoc Mol Biol. 2015;111(1):31–2.

1000 52. Port F, Bullock SL. Augmenting CRISPR applications in Drosophila with tRNA-flanked
1001 sgRNAs. Nat Methods. 2016;13(10):852–4.

1002 53. Cunningham F, Allen JE, Allen J, Alvarez-Jarreta J, Amode MR, Armean IM, et al.
1003 Ensembl 2022. Nucleic Acids Res. 2022;50(D1):D988–95.

1004 54. DeLuca SZ, Spradling AC. Efficient expression of genes in the Drosophila germline
1005 using a UAS promoter free of interference by Hsp70 piRNAs. Genetics.
1006 2018;209(2):381–7.

1007 55. Vazquez-Pianzola P, Adam J, Haldemann D, Hain D, Urlaub H, Suter B. Clathrin heavy
1008 chain plays multiple roles in polarizing the Drosophila oocyte downstream of Bic-D.
1009 Development. 2014;141(9):1915–26.

1010 56. Cox J, Mann M. MaxQuant enables high peptide identification rates, individualized
1011 ppb-range mass accuracies and proteome-wide protein quantification. Nat
1012 Biotechnol. 2008;26(12):1367–72.

1013 57. Consortium U. UniProt: a worldwide hub of protein knowledge. Nucleic Acids Res.
1014 2019;47(D1):D506–15.

1015 58. Huber W, Von Heydebreck A, Sültmann H, Poustka A, Vingron M. Variance
1016 stabilization applied to microarray data calibration and to the quantification of
1017 differential expression. Bioinformatics. 2002;18(suppl_1):S96–104.

1018 59. Silva JC, Gorenstein M V, Li GZ, Vissers JP. C; Geromanos, SJ Absolute quantification of
1019 proteins by LCMSE: A virtue of parallel MS acquisition. Mol Cell Proteomics.
1020 2006;5:144–56.

1021 60. Silver JD, Ritchie ME, Smyth GK. Microarray background correction: maximum
1022 likelihood estimation for the normal–exponential convolution. Biostatistics.
1023 2009;10(2):352–63.

1024 61. Kammers K, Cole RN, Tiengwe C, Ruczinski I. Detecting significant changes in protein
1025 abundance. EuPA open proteomics. 2015;7:11–9.

1026 62. Uldry A-C, Maciel-Dominguez A, Jornod M, Buchs N, Braga-Lagache S, Brodard J, et al.
1027 Effect of Sample Transportation on the Proteome of Human Circulating Blood
1028 Extracellular Vesicles. Int J Mol Sci. 2022;23(9):4515.

1029 63. Andrews S. FastQC: a quality control tool for high throughput sequence data.
1030 Babraham Bioinformatics, Babraham Institute, Cambridge, United Kingdom; 2010.

1031 64. Wang L, Wang S, Li W. RSeQC: quality control of RNA-seq experiments.
1032 Bioinformatics. 2012;28(16):2184–5.

1033 65. Smith T, Heger A, Sudbery I. UMI-tools: modeling sequencing errors in Unique
1034 Molecular Identifiers to improve quantification accuracy. Genome Res.
1035 2017;27(3):491–9.

1036 66. Martin M. Cutadapt removes adapter sequences from high-throughput sequencing
1037 reads. EMBnet J. 2011;17(1):10–2.

1038 67. Kim D, Langmead B, Salzberg SL. HISAT: a fast spliced aligner with low memory
1039 requirements. Nat Methods. 2015;12(4):357–60.

1040 68. Liao Y, Smyth GK, Shi W. featureCounts: an efficient general purpose program for
1041 assigning sequence reads to genomic features. Bioinformatics. 2014;30(7):923–30.

1042 69. Love MI, Huber W, Anders S. Moderated estimation of fold change and dispersion for
1043 RNA-seq data with DESeq2. Genome Biol. 2014;15(12):1–21.

1044 70. Core R. TEAM, 2017. R: A language and environment for statistical computing. R
1045 Foundation for Statistical Computing, Vienna, Austria. Online https//www r-project
1046 org. 2022;

1047 71. Castells-Nobau A, Nijhof B, Eidhof I, Wolf L, Scheffer-de Gooyert JM, Monedero I, et
1048 al. Two algorithms for high-throughput and multi-parametric quantification of
1049 Drosophila neuromuscular junction morphology. J Vis Exp Jove. 2017;(123).

1050 72. Szklarczyk D, Franceschini A, Wyder S, Forslund K, Heller D, Huerta-Cepas J, et al.
1051 STRING v10: protein–protein interaction networks, integrated over the tree of life.
1052 Nucleic Acids Res. 2015;43(D1):D447–52.

1053 73. Stoll G, Pietiläinen OPH, Linder B, Suvisaari J, Brosi C, Hennah W, Leppä V, Torniainen
1054 M, Ripatti S, Ala-Mello S, Plöttner O, Rehnström K, Tuulio-Henriksson A, Varilo T,
1055 Tallila J, Kristiansson K, Isohanni M, Kaprio J, Eriksson JG, Raitakari OT, Lehtimäki T,
1056 Jarvelin MR, Salomaa V, Hurles M, Stefansson H, Peltonen L, Sullivan PF, Paunio T,
1057 Lönnqvist J, Daly MJ, Fischer U, Freimer NB, Palotie A. Deletion of TOP3β, a
1058 component of FMRP-containing mRNPs, contributes to neurodevelopmental
1059 disorders. Nat Neurosci. 2013 Sep;16(9):1228-1237. doi: 10.1038/nn.3484. Epub 2013
1060 Aug 4. PMID: 23912948; PMCID: PMC3986889.

1061 74. Su, S, Xue, Y., Sharov, A., Zhang, Y., Lee, S.K., Martindale, J.L., Li, W., Ku, W.L., Zhao, K.,
1062 De, S., Shen, W., Sen, P., Gorospe, M., Xu, D., Wang, W. A dual-activity topoisomerase
1063 complex regulates mRNA translation and turnover. Nucleic Acids Res
1064 2022;50(12):7013-7033.

1065 75. Schiavo G, Greensmith L, Hafezparast M, Fisher EM. Cytoplasmic dynein heavy chain:
1066 the servant of many masters. Trends Neurosci. 2013 Nov;36(11):641-51. doi:
1067 10.1016/j.tins.2013.08.001.

1068 76. Wilkie GS, Davis I. Drosophila wingless and pair-rule transcripts localize apically by
1069 dynein-mediated transport of RNA particles. Cell. 2001 Apr 20;105(2):209-19.
1070 doi: 10.1016/s0092-8674(01)00312-9. PMID: 11336671.

1071 77. Bullock SL, Ish-Horowicz D. Conserved signals and machinery for RNA transport in
1072 Drosophila oogenesis and embryogenesis. Nature. 2001 Dec 6;414(6864):611-6.
1073 doi: 10.1038/414611a. PMID: 11740552.

1074 78. Goodman, L.D., Prudencio, M., Srinivasan, A.R., Rifai, O.M., Lee, V.M., Petrucelli, L.,
1075 Bonini, N.M. (2019). eIF4B and eIF4H mediate GR production from expanded G4C2 in a
1076 Drosophila model for C9orf72-associated ALS. Acta Neuropathol. Commun. 7(1): 62.